Abstract

Title of Thesis: MODELING OF MINERAL TRAPPING FOR CO_2 SEQUESTRATION

Mohammad Alizadeh Nomeli, MS, 2011

Thesis Directed By: Advisor: Dr. Amir Riaz

Co-advisor: Dr. Alba Torrents

Department of Civil and Environmental Engineering

In order to prevent CO_2 concentrations in the atmosphere from rising to unacceptable levels, carbon dioxide is sequestered beneath the ground surface. CO_2 can be trapped as a gas under a low-permeable cap rock (structural trapping) or can dissolve into the ground water (hydrodynamic trapping); it can also react with minerals and organic matter that are dissolved in the brine to form precipitates (mineral trapping). From the perspective of secure, long term storage, mineral trapping has been identified as the most effective mechanism related to subsurface sequestration. Temperature, pressure and salinity are among the primary parameters governing the overall behavior of the process of mineral trapping. In this study, the primary goal is to simulate the behavior of carbon dioxide with an improved model under the conditions of temperature and pressure typical of saline aquifers, i.e. 50 to 100˚C and 1-500 bar, respectively. The objective is to determine how the related quantities of molar volume as well as CO_2 fugacity change in response to changes in pressure and temperature so that the associated changes in the solubility and the precipitation of carbonates, indicating the rate of CO_2 consumption, can be quantified. This study finds that the dissolution rate of anorthite and the rate of precipitation of calcite both rise with the increase in pressure and temperature. The dissolution rate of anorthite has been found to be the rate-limiting process in the sequestration of CO_2 and governs the consumption rate of CO_2 in the aqueous phase. These results show good agreement with those obtained from experimental work reported in other studies. This study also agrees earlier findings based on relatively less precise models, with respect to the increase in CO_2 solubility at higher pressures and a decrease in solubility associated with increasing values of temperature and salinity.

SIMULATION OF MINERAL TRAPPING FOR CO_2 SEQUESTRATION

by

Mohammad Alizadeh Nomeli

Thesis submitted to the faculty of the Graduate School of the

University of Maryland, College Park in partial fulfillment

of the requirements for the degree of

Master of Science

2011

Advisory Committee:

Assistant Professor Amir Riaz

Professor Alba Torrents

Professor Allen P. Davis

DEDICATION

To my loving parents, Manizheh and Hossein who have never left my side and always hold a special place in my heart.

To my sisters Maedeh and Mahdieh for their unconditional love, guidance, and support.

ACKNOWLEDGEMENT

I wish to thank my supervising professor, Dr. Amir Riaz for his patience, motivation, enthusiasm, guidance, support, advice and immense knowledge. He showed me the transcendent way of research and filled my graduate experience with a plenty of joy. I always admire his insight to understand and analyze unexpected problems.

I also want to show my deep gratitude to my committee Professor Alba Torrents and Professor Allen P. Davis for their encouragement and insightful comments. Their advices and suggestions have given me a thorough understanding about this work and led me here with excellent intuition.

I am indebted to Professor Dr. Santiago Solares for the numerous interesting conversations, which have helped to clarify my understanding of several aspects.

I am grateful to Dr. Ali Rassoulpour, Barbara Varsa and Joanne Desiato for their support.

I thank my fellow labmate, Don Daniel for the stimulating discussions and for all the fun we have had.

This work would not have been possible without the encouragement of my dear friends.

Last but not the least; I would like to thank my parents Manizheh and Hossein, for giving birth to me at the first place and supporting me spiritually throughout my life.

Table of Contents

List of Figures

List of Tables

Chapter 1: Introduction

1.1. Overview

It is now widely recognized that global warming is a direct consequence of increased levels of the concentration of CO_2 in the atmosphere which are about 30% higher compared to the pre-industrial era [3]. Higher concentrations of CO_2 lead to increased trapping of infrared radiations emitted from the Earth's surface. Arguably, more than half of this increase in infrared absorption is due to the behavior of CO_2 as a greenhouse gas [4]. In order to avoid the negative consequences of an unchecked increase in global warming produced by the continued emissions of CO_2, several strategies have to be undertaken to decrease the concentration in the atmosphere. While a reduction in the consumption of green house gas producing substances, such as fossils fuels, is considered an essential first step in the control of global warming, other solutions for handling excess emissions such as the long-term sequestration of CO_2 in the subsurface formations are necessary. Several scientific and technical challenges (discussed in §1.2) need to be addressed in order to advance sequestration from a promising concept to a safe, viable and effective strategy for the containment of global warming [2].

Among the main natural reservoirs of carbon are the oceans, that store about $38{,}000 \times 10^{15}\ g\ C$ (gram of carbon), and terrestrial soils, with a capacity of about $15{,}000 \times 10^{15}\ g\ C$. Terrestrial plants and the atmosphere are relatively smaller reservoirs with capacities of $\sim 500 \times 10^{15}\ g\ C$ and $\sim 730 \times 10^{15}\ g\ C$, respectively [2]. The net exchange of carbon dioxide between the atmosphere and the ocean surface is $\sim\ 90 \times 10^{15}\ g\ C\ a^{-1}$(gram of carbon per contact surface area). At present, the biologically driven carbon cycle in the oceans is close to steady state [35, 38]. Experiments have shown that the overall productivity of the ocean is not controlled by CO_2 concentrations, apart from few exceptions [1]. Furthermore, the ratios of limiting nutrients and dissolved inorganic carbon (DIC) in deep ocean are close to the so-called Redfield ratios [82]. Hence, it is virtually impossible to increase the consumption rate rate of CO_2 from the atmosphere through the process of photosynthesis [1].

Sequestration of CO_2 through injection into deep geological aquifers has emerged as the most viable long-term storage option [5]. Numerous field studies have been carried out to determine the

optimal conditions for the injection of CO_2. Currently sequestration in saline aquifers composed of sandstone and carbonate formations in sedimentary basins is favored due to their chemical structure, porosity and temperature and pressure conditions that promote natural occurrence of the three primary processes of sequestration; capillary, solubility and mineral trapping [6]. The depths of these deep saline aquifers range from 800 to 2000m. While the typical thickness of an aquifer is small, in the range of 100-200 meters, the horizontal extant can be spread over several kilometers [7]. Based on the surface temperature and the geothermal temperature gradient, that varies between 20-60°C/km, temperatures and pressures within the aquifer can range, respectively, from 25°C to 200°C and from 10bar to 100bar [8]. The pressure and temperature conditions therefore do not change appreciably within a single aquifer. Consideration of the CO_2 phase behavior indicates that CO_2 exists in a supercritical state under suitable aquifer conditions where its density and viscosity vary, respectively, between 266 to 766 kg/m^3 and 0.03 to 0.05mPa-s [9]. The density and viscosity of the formation brines, accounting for the typical range of salt and mineral concentrations, range from 998 to 1230 kg/m^3 and 0.195 to 1.58mPa-s, respectively [7]. Both the density and viscosity of brine are greater than those of supercritical CO_2[10].

Within brine aquifers, CO_2 is expected to be trapped mainly by the following three physical mechanisms:

Capillary trapping refers to the process of immobilization of CO_2 in microscopic pores of the geologic formation through the action of capillary forces. Because the supercritical CO_2 does not wet the surface of the rock, small quantities are left trapped inside the pores, surrounded by the wetting brine phase, as the CO_2 drains locally due to its positively buoyant state [15].

Solubility trapping refers to the process of dissolving CO_2 in the aquifer brine. Dissolution takes place at the CO_2/brine interface where the rate of dissolution is controlled by a complex interaction of thermodynamic, chemical and hydrodynamic mechanisms. Thermodynamic conditions of pressure, temperature and solution density as well as chemical composition of dissolved salts and minerals in the brine govern the solubility of CO_2 with respect to brine. Accelerated dissolution takes place due to the process of natural convection which occurs as a

result of the increase in the density of saturated brine (solution of brine and aqueous CO_2) [22]. This hydrodynamic instability gives rise to negatively buoyant plumes of saturated brine within an environment of unsaturated brine [14] that are responsible for switching the rate of dissolution from a diffusive to a convective basis. The process of natural convection significantly increases the amount of CO_2 dissolved over long periods of time compared to the amount dissolved by diffusion alone [23] in the absence of natural convection.

Mineral trapping is associated with the formation of solid precipitates of carbonates by the chemical reaction among the dissolved CO_2 and the calcium available in typical aquifer rocks such as anorthite. Depletion of dissolved CO_2 from brine through calcite formation lowers the local concentration of dissolved CO_2, which affects the behavior of hydrodynamic instability, which in turn affects the rate of dissolution across the CO_2/brine interfaces.

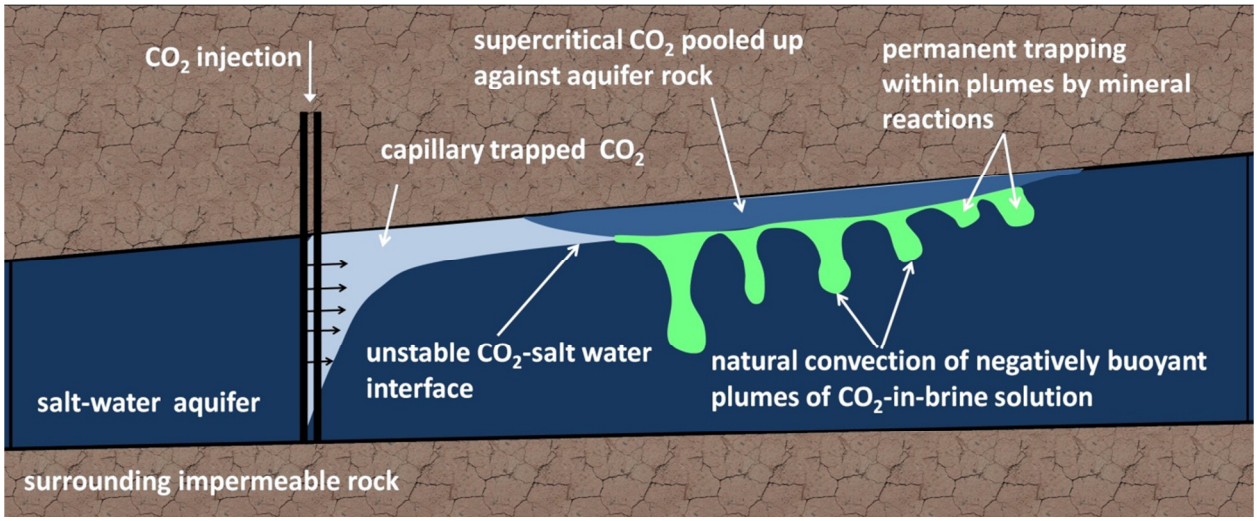

Figure 1. Schematic representation of the capillary trapping, solubility trapping and mineral trapping of CO_2.

In figure 1, after injection of CO_2 under the low permeable cap rock at high pressure and temperature, it goes to supercritical phase and pools up above the aquifer. It also creates an unstable rich-CO_2 boundary layer above the brine. This then starts propagating downward as fingers. Chemical reactions take place at the interface between the fingers and the brine which in turn leads to a permanent source of trapping within the plumes. Mineral trapping within the plumes is limited by various conditions: (1) the mineral composition contents; (2) the water content. When either one of the two runs out, the process will come to a halt or new equilibrium

will be established. However, excess carbon dioxide will strongly influence this equilibrium as well as the precipitation of carbonate, because the dissolution of CO_2 results in acidification of the system.

Although there are basic unresolved problems in all three areas noted above, this study would be directed towards developing a fundamental understanding of the thermodynamic basis of solubility as well as quantifying the relevant reaction kinetics associated with mineralization in saline aquifers. These two processes play a pivotal role in the overall process of CO_2 sequestration both by promoting enhanced solubility through natural convection as well as by facilitating a stable form of trapping through carbonate precipitation. In the following, we discuss the outstanding issues in each of these areas to help frame our objectives in §1.2 followed by a discussion of our methodology for addressing these issues in §1.3.

Chapter 2: Objective and methodology

2.1. Objective

The principle objective of this study is to determine the mineral precipitation rate associated with the process of CO_2 sequestration in deep saline aquifers. The focus is on obtaining the rate of mineral precipitation by combining the thermodynamics of the dissolution process with the reaction kinetics of mineral trapping, under typical saline aquifers conditions. In order to find the mineral precipitation rate, it is necessary to know the rate of dissolution of CO_2 into brine. This has been characterized for aquifer parameters of pressure, temperature, salinity and pH [24]. However, earlier attempts to quantify the rate of dissolution as a function of aquifer parameters have relied mainly on the experimental determination of activity coefficients that govern the behavior of dissolution [25]. Moreover, most of the earlier works on finding the precipitation rate of minerals have also been experimental in nature [26]. In contrast, in this work, all relevant solubility and kinetic are calculated using fundamental thermodynamic principles. Hence, this work provides a theoretical basis for quantifying a wide range of experimental data relevant to saline aquifers that will further facilitate a coherent integration of the processes of solubility and mineralization with those related to hydrodynamic instability.

2.2. Methodology

As can be seen in figure 2 the setup considered in this work consists of a two-phase region where a CO_2-rich (supercritical) phase [39] and the H_2O-rich liquid brine phase coexist and are mutually soluble [36, 48]. Dissolution across the interface can be characterized at a given pressure and temperature by applying an appropriate solubility model for determining the partitioning between the aqueous and gas phases [6, 12]. Subsequent chemical reactions in the aqueous phase leading to the dissociation of carbonic acid are fast and can therefore be treated as equilibrium reactions [27]. Because precipitation involves relatively slower reactions between the components of dissociated dissolved CO_2 and minerals in the brine, we need to take into account the kinetics of these reactions, such as reaction order and rate constants [28].

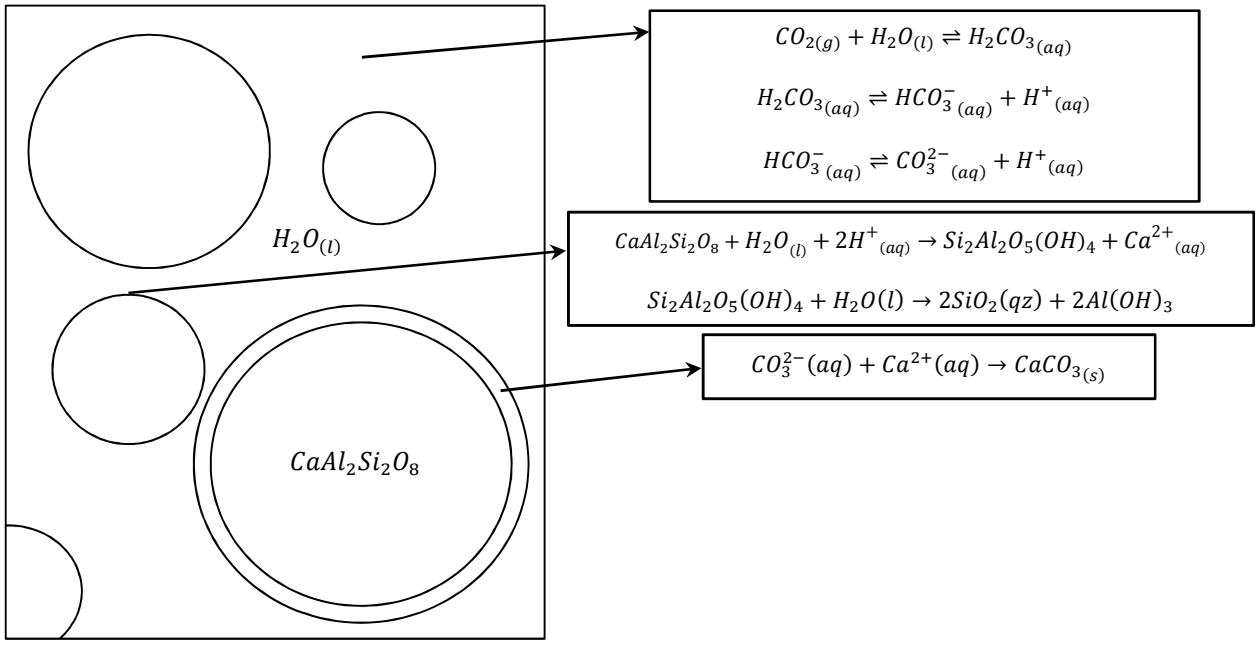

Figure 2 shows the reactions occurring during the dissolution of anorthite. The protons formed by the CO_2-dissolution will attack the anorthite, resulting in the release of Ca^{2+}-ions. The calcium and bicarbonate or carbonate ions will together result in the precipitation of calcite.

Characterization of equilibrium constants for aqueous reactions as well as rate constants and reaction orders for precipitation reactions involves the determination of how the quantities of molar volume and fugacity of CO_2 change in response to changes in pressure and temperature and affect the processes of solubility and precipitation. The latter process is responsible for setting the rate of CO_2 consumption because precipitation of CO_2 as a calcite ($CaCO_3$) causes a corresponding decrease in the mass of CO_2 in the aqueous phase. Actually, variations in the precipitation of secondary carbonate minerals strongly depend on rock mineral composition and their kinetic reaction rates.

The variation of molar volume and fugacity of CO_2 in response to the change in pressure and temperature can be calculated by applying the Redlich-Kwong [11] and related equations [61]. The molar volumes recommended by NIST agree with those obtained with the modified Redlich-Kwong equation [60]. We determine the values of activity coefficients of CO_2 based on the molar volumes determined through the modified Redlich-Kwong equation [60]. In previous works, the researchers used experimental data to obtain the activity coefficients of CO_2 in saline aquifers [33, 39]. In this study, the activity coefficients of CO_2 are calculated based on the fugacity of CO_2

calculated through the corresponding values of molar volume and thermodynamic equilibrium constants. We show how these changes affect solubility and the precipitation of CO_2 in the liquid phase and allow the measurement of the rate of CO_2 consumption. As long as the equilibrium reactions between each secondary species and the basis have been considered, any reaction written among the secondary species is redundant in order to find the consumption rate of CO_2 [13, 34]. Furthermore, geochemical reaction path modeling, tracing the change of aqueous solution compositions and speciation and minerals through time or reaction progress, has been used to assess the extent of water-aqueous-gas interactions under reservoirs conditions with appropriate ranges of temperature and pressure. According to the United States Geological Surveys (USGS) [46] respective parameters conforming to a general Arrhenius-type rate equation is applied to find the dissolution and precipitation rates.

The method is implemented in a computer routine using FORTRAN, to model (1) the CO_2-H_2O mixture by applying the new Redlich-Kwong parameters, and (2) aqueous solubility for gaseous and liquid CO_2 as a function of temperature, pressure and salinity (3) precipitation and dissolution rates of minerals in aquifers as a function of temperature, pressure and pH of the system. The results are compared with experiments at each step. Differences between experimental and calculated results may arise due to factors not accounted for in the theoretical model including, i.e. variations in grain size, aquifer heterogeneity, primary and secondary mineral coatings, and secondary minerals that may lead to decreased porosity and permeability [10]. However, for the most part, mutual solubilities and the consumption rate of CO_2 in liquid phase reported by various sources are in good agreement with the results in this method.

2.3. Concluding remarks

Injection of CO_2 in deep oceanic waters might temporarily reduce atmospheric CO_2 concentrations, but it is not a final solution. In addition, it represents, at least for the time being, an insurmountable technological challenge and involves high environmental risks related to sudden release of CO_2. Sequestration of CO_2 through injection into deep geological reservoirs and mineral carbonation represents two other options: (1) trapping as gas or supercritical fluid below a low-permeable caprock, (2) precipitation of secondary carbonates. The last process or

mineral trapping is especially attractive as the virtually permanent CO_2 fixation in form of carbonates into relatively deep geological formations prevents its return to the atmosphere.

The following chapters are dedicated to the reactants, i.e. CO_2 and products, i.e. the carbonate minerals, their thermodynamic properties and the kinetics of relevant dissolution and precipitation reactions.

Chapter 3: Behavior of CO_2 in supercritical and liquid phase

3.1. The geological sequestration of CO_2

The scope of this stage is to find the behavior of CO_2 after injection at high pressure into a system made up of a relatively deep aquifer that has an aqueous solution with high molality of salinity. First step, pressure and temperature can be calculated from the pressure gradient and geothermal gradient. According to the average geothermal gradient of $33^oC\ km^{-1}$, and hydrostatic gradient of $100\ bar\ km^{-1}$, a depth of 1 km the temperature and pressure will be 48^oC and $101\ bar$ [8]. Under this condition a CO_2-rich gas or liquid phase and an H_2O-rich liquid phase exist together. The effect of salinity on the mutual solubility of CO_2 and H_2O also needs to be taken into account in addition to reactions between fluids and aquifer rocks.

3.2. The vapor-liquid curve equation

In thermodynamics, the triple point of a substance is the temperature and pressure at which three phases for example, gas, liquid and solid coexist in thermodynamic equilibrium. The critical point is used to denote the specifically the vapor-liquid critical point of a substance. The supercritical phase is above the critical point whereas distinct liquid and gas phases do not exist. The triple point of CO_2 is at -56.57 ± 0.03^oC and 5.185 ± 0.005 bar [83] and the critical point is 30.978 ± 0.015^o [84] Recent critical pressure estimate is 73.773 ± 0.003 bar [9, 71]. The vapor-liquid curve equation extending from the triple point to the critical point with sufficient accuracy (typically<0.4%) is:

$$\log P_{sat} = \frac{-863.6}{T_{sat}} + 4.705 \qquad 3\text{-}1$$

where, P_{sat} is the vapor pressure in bar and T_{sat} is in Kelvin [84]:

Melting curve (solid-liquid curve) is:

$$P_{melt} = 523.18 - 51.547\ T_{melt} + 0.22695\ T_{melt}^2 \qquad 3\text{-}2$$

where, P_{melt} is in bar and T_{melt} is in Kelvin.

Table 1 shows the typical aquifer conditions.

Typical aquifer conditions	Temperature(°C)	Pressure(bar)	Salinity(molality)	pH
	50-100	1-500	0-3	<6.5

Table 1 shows the typical aquifer conditions i.e. temperature, pressure, salinity, pH, etc. The hydrostatic pressure covered in this study is 74-500 MPa, and the temperature is in the range of 323-373 K. According to the critical point of CO_2 it is obvious that CO_2 is a supercritical fluid under most pressure and temperature conditions in the sequestrating of carbon [9].

3.3. Equation of state

According to the ideal gas law (Benoit Paule Emile Clapeyron, 1834), there is a relationship between pressure, temperature and volume of the fluid: [10]

$$P = \frac{RT}{v} \qquad 3\text{-}3$$

where v stands for the molar volume of a gas and R is the universal gas constant.

According to the definition of an ideal gas, it is made up of infinitesimally small particles that do not interact with one another. This condition is approached by real gases at low pressure and high temperature. But under the reservoir conditions the ideal gas law is not applicable; therefore we should use alternative EOS for real gases. For example according to van der Waals (1873) and Rowlinson (1988) this relationship can be expressed by following equation:

$$P = \frac{RT}{v-b} - \frac{a}{v^2} \qquad 3\text{-}4$$

where, a and b are correcting terms. The parameter b is the effective volume of the molecules contained in a mole of gas, and the difference $(v-b)$ represents the volume available for the movements of gas molecules, in other words the unoccupied or free volume per mole. The second term on the right-hand side of equation (3-4) is a correction for intermolecular attractions.

Another form of EOS was expressed by Redlich and Kwong (1949):

$$P = \frac{RT}{v-b} - \frac{a}{T^{0.5}v(v+b)} \quad 3\text{-}5$$

In a modified Redlich-Kwong EOS (3-5) of Kerrick and Jacobs (1981) with different coefficients for the supercritical range, *b* is constant and equal to 29.0 cm^3mol^{-1}, whereas *a* is a function of both *T* and *V*. Equation (3-5) fits the NIST (National Institute of standards and technology) data for molar volume of CO_2 (figure 4) [11].

The Redlich-Kwong EOS was further modified to explain the properties of CO_2 at elevated pressures and temperatures. For instance, the modified Redlich-Kwong EOS of Kerrick and Jacobs (1981) as follows:

$$P = \frac{RT(1+y+y^2-y^3)}{v(1-y)^3} - \frac{a}{T^{0.5}v(v+b)} \quad 3\text{-}6$$

where:

$$y = \frac{b}{4v} \quad 3\text{-}7$$

$$a(T,v) = c + \frac{d}{v} + \frac{e}{v^2} \quad 3\text{-}8$$

$$c = (290.78 - 0.30276\,T + 0.0014774\,T^2) \times 10^6\ bar\ cm^2\ K^{0.5}\ mol^{-2} \quad 3\text{-}9$$

$$d = (-8374 + 19.437\,T - 0.008148\,T^2) \times 10^6\ bar\ cm^3\ K^{0.5}\ mol^{-3} \quad 3\text{-}10$$

$$e = (76600 - 133.9\,T + 0.1071\,T^2) \times 10^6\ bar\ cm^4\ K^{0.5}\ mol^{-4} \quad 3\text{-}11$$

Table 2. shows the values for b, c, d and e at 25, 50, 75 and 100°C.

Temperature(°C)	b	c	d	e
25	29.0	331.757×10^6	-3305.349×10^6	46208.7×10^6
50	29.0	347.124×10^6	-2945.922×10^6	44523.9×10^6
75	29.0	364.339×10^6	-2596.679×10^6	42973.04×10^6
100	29.0	383.400×10^6	-2257.622×10^6	41556.02×10^6

The *a* and *b* parameters of the van der Waals and Redlich-Kwong EOS can be accurately estimated by fitting the available *P-T-v* data for the considered gas [9]. Alternatively, they can be obtained from the *P-T-v* data at the critical point [11]. The critical isotherm is horizontal at the critical point, which also represents an inflation point of the critical isotherm, so both the first and second partial derivatives of *P* with respect to *V*, at constant *T*, are equal to zero.

For van der Waals: [33]

$$P_c = \frac{RT_c}{v_c - b} - \frac{a}{{v_c}^2} \qquad 3\text{-}12$$

$$\begin{cases} \left(\frac{\partial P}{\partial v}\right)_{T_c} = \frac{-RT_c}{(v_c - b)^2} + \frac{2a}{v_c^3} = 0 \\ \left(\frac{\partial^2 P}{\partial v^2}\right)_{T_c} = \frac{2RT_c}{(v_c - b)^3} - \frac{6a}{v_c^4} = 0 \end{cases} \rightarrow \quad a = \frac{27\, R^2 T_c^2}{64\, P_c} \quad , \quad b = \frac{RT_c}{8\, P_c} \qquad 3\text{-}13$$

Same procedure to the Redlich-Kwong equation yields:

$$a = 0.4275\, \frac{R^2 T_c^{2.5}}{P_c} \quad , \quad b = 0.0866\, \frac{RT_c}{P_c} \qquad 3\text{-}14$$

3.4. Molar volume of CO_2

Molar volume can be calculated by substituting *a* and *b* obtained from equation (3-13) and (3-14) into the equation (3-12). Therefore van der Waals and Redlich-Kwong equation can be expressed by following equations:

$$v^3 - \left(b + \frac{RT}{P}\right) v^2 + \left(\frac{a}{P}\right) v - \frac{ab}{P} = 0 \qquad 3\text{-}15$$

$$v^3 - \frac{RT}{P} v^2 - \left(\frac{RTb}{P} - \frac{a}{T^{0.5} P} + b^2\right) v - \frac{ab}{T^{0.5} P} = 0 \qquad 3\text{-}16$$

The minimum root gives the molar volume of the liquid phase whereas the molar volume of the gas phase (or better of the vapor phase) is given by the maximum root (Spycher et al., 2003).

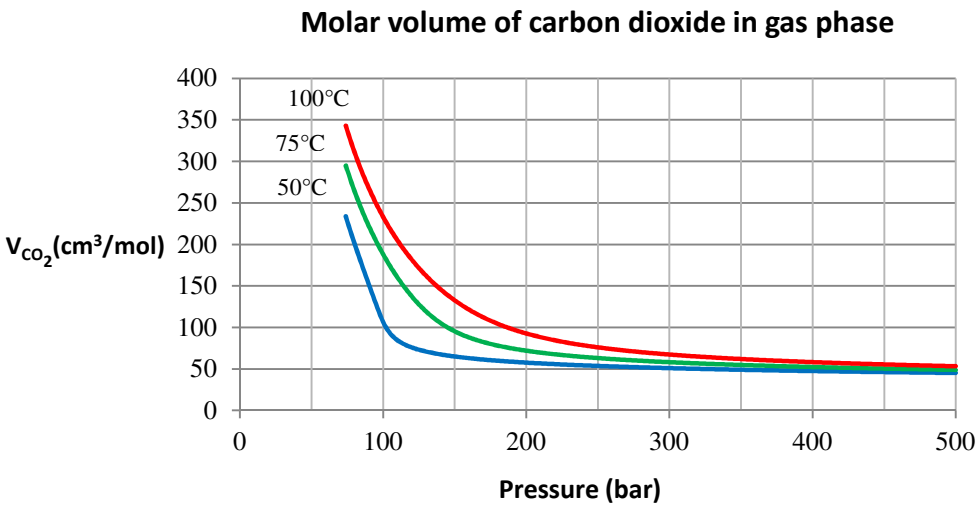

Figure 3. Shows the molar volume of CO_2 computed by Redlich-Kwong equation.

Figure 3 depicts the variation of molar volume of carbon dioxide with the pressure in reservoir conditions (a temperature range of 50 to 100˚C and a pressure range of 74 to 500 bar). As we can see, molar volume of CO_2 initially decreases rapidly with increase in pressure and then, at higher pressures, molar volume varies slowly in response to the change in pressure. On the other hand, at higher temperatures, CO_2 is found to occupy higher volume.

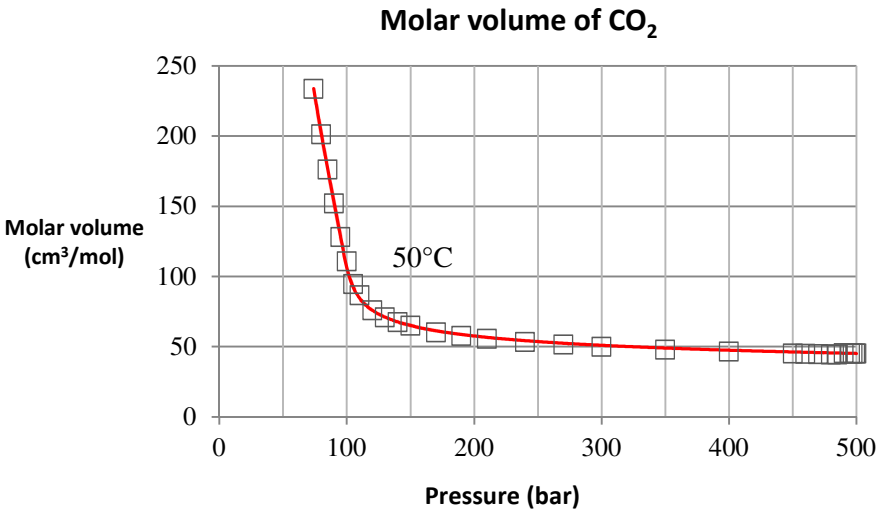

Figure 4. The molar volume of CO_2 computed by Redlich-Kwong equation (line) and molar volumes recommended by NIST (data from Lemmon et al., 2003) are shown (squares).

Figure 4 depicts the variation of molar volume of carbon dioxide at 50°C with the pressure in reservoir conditions (a pressure range of 74 to 500 bar). As can be observed, the molar volumes recommended by NIST (Lemmon et al., 2003) are satisfactory fitted by the Redlich-Kwong equation.

3.5. Density of CO_2

Since the molar volume of carbon dioxide is known, the density ρ is readily calculated:

$$\rho = \frac{MW}{v} \qquad 3\text{- }17$$

where, MW is molecular weight of CO_2.

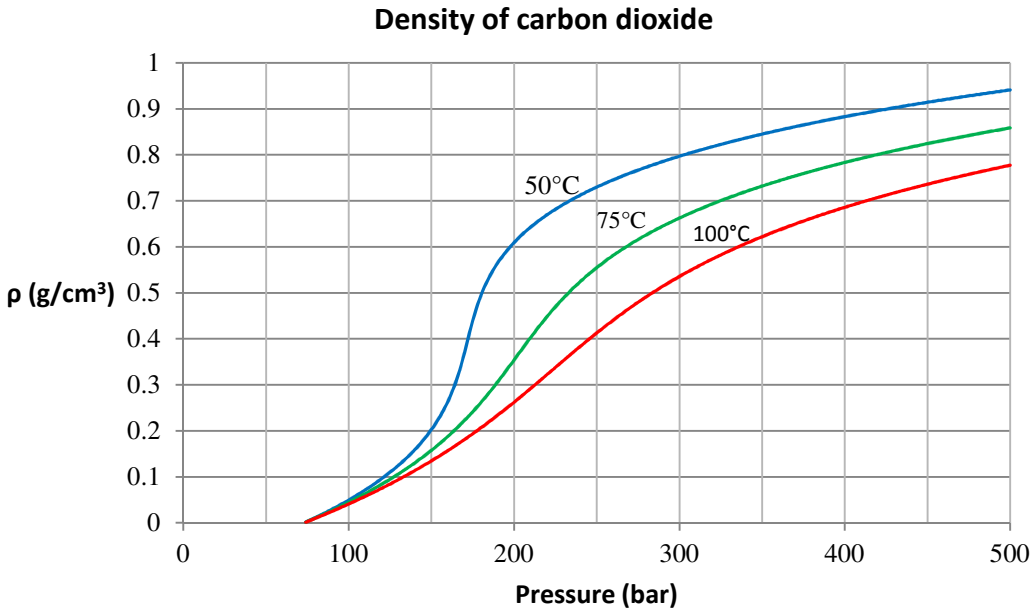

Figure 5. Density of CO_2 computed at different temperatures and variable pressures by means of the Redlich-Kwong equations.

Figure 5 depicts the variation of density of carbon dioxide with the pressure in reservoir conditions (a temperature range of 50 to 100˚C and a pressure range of 74 to 500 bar). At lower temperatures, it can be observed a sharp increase in the density of CO_2 with increase of pressure.

However, at higher temperatures, it is seen that density varies gradually in response to the change in pressure.

3.6. Compressibility factor

Compressibility factor Z is defined in order to magnify the deviations from ideality (For a perfect gas Z=1):

$$Z = \frac{Pv}{RT} \qquad 3\text{- }18$$

At high pressures molecules are colliding more often. This allows repulsive forces between molecules to have a noticeable effect, making the volume of the real gas (V_{real}) greater than the volume of an ideal gas (V_{ideal}) which causes Z to increase above one. In reservoirs pressures range (up to 500 bar), the molecules are more free to move. In this case attractive forces dominate, making $Z < 1$ [62].

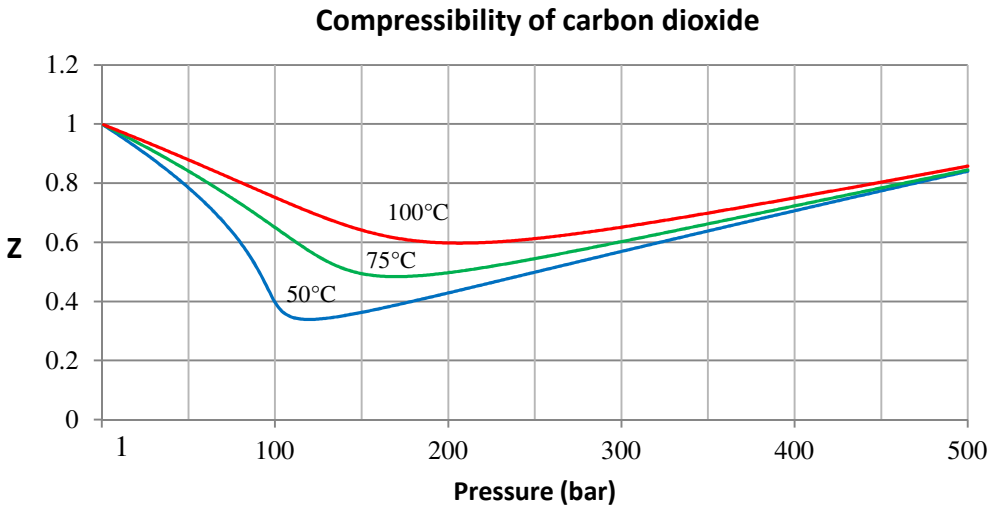

Figure 6. Compressibility factor of CO_2 computed at different temperatures and pressures by means of Redlich-Kwong equation.

Figure 6 depicts the variation of compressibility of carbon dioxide with the pressure in reservoir conditions (a temperature range of 50 to 100˚C and a pressure range of 74 to 500 bar). The compressibility of CO_2 has been found to decrease and reach a well. The well is deeper at lower

temperatures and gradually increases with increase in temperature and pressure. The closer the gas is to its critical point or its boiling point, the more *Z* deviates from the ideal case. Above the 100 bar Redlich-Kwong is more in agreement with NIST than van der Waals [1].

From what have been observed in above figures, density changes are directly related to changes in molar volume during the sequestration of CO_2. Carbon dioxide injected into aquifers moves upwards because of buoyancy caused by the density differences between CO_2 and formation water, except for aquifers at high pressure and low temperature. CO_2 compressibility effects may play an important role in determining the size and geometry of the CO_2 plume that will develop when supercritical CO_2 is injected in an aquifer.

3.7. Fugacity coefficient of CO_2

Fugacity coefficient of CO_2 is also defined to find the deviations from ideal condition (Appendix 1):

$$\ln \emptyset = \ln \frac{f}{P} = \frac{1}{RT}(\mu_i - \mu_i^o) = \frac{1}{RT}\left(-\int_{Tr}^{T} s_k dT + \int_{Pr}^{P} v_k dP\right) = \frac{1}{RT}\int_{P\to 0}^{P}\left(v - \frac{RT}{P}\right)dP$$

$$= \frac{1}{RT}\int_{0}^{P}\left(\frac{ZRT}{P} - \frac{RT}{P}\right)dP = \int_{0}^{P}\frac{Z-1}{P}dP$$

$$\ln \emptyset = \int_{0}^{P}\frac{Z-1}{P}dP \qquad 3\text{- }19$$

Here, *Z* is compressibility factor; *P* is pressure and $\emptyset$ is fugacity coefficient. As can be seen the fugacity coefficients decrease with increasing pressure. For real gases only at very low total pressures the following equation (3-18) is reasonable:

$$f_i = P_i = y_i\, P_{total} \qquad 3\text{- }20$$

In other words, for real gases only at very low total pressures, $\emptyset = \mathbf{1}$. Here, the fugacity of the *i*th gaseous component is equal to its partial pressure $\boldsymbol{P_i}$.

3.8. Fugacity coefficient of H_2O and CO_2 in H_2O-CO_2 mixtures

In general equation (3-21) is applied to compute fugacity coefficients in the CO_2-rich phase:

$$\ln \emptyset_k = \ln\left(\frac{v}{v - b_{mix}}\right) + \frac{b_k}{v - b_{mix}} - \frac{2\sum_{i=1}^{n} y_i a_{ik}}{b_{mix} RT^{3/2}} \ln\left(\frac{v + b_{mix}}{v}\right) + \frac{a_{mix} b_k}{b_{mix}^2 RT^{3/2}} \left[\ln\left(\frac{v + b_{mix}}{v}\right) - \frac{b_{mix}}{v + b_{mix}}\right] - \ln Z \quad \text{3- 21}$$

where, *i* and *k* are the components in the mixture, for example water and CO_2. It is reasonable to assume infinite H_2O dilution in the CO_2-rich phase [85]. Under the hypothesis of infinite H_2O dilution in the CO_2-rich phase, equations (3-22) and (3-23) reduce to the equation (3-24) for CO_2:

$$b_{mix} = y_{CO_2} b_{CO_2} + y_{H_2O} b_{H_2O} \quad \text{3- 22}$$

$$a_{mix} = y_{CO_2}^2 a_{CO_2} + 2 y_{H_2O} y_{CO_2} a_{H_2O-CO_2} + y_{H_2O}^2 a_{H_2O} \quad \text{3- 23}$$

$$b_{mix} = b_{CO_2} \quad , \quad a_{mix} = a_{CO_2} \quad \text{3- 24}$$

Therefore, under the hypothesis of infinite H_2O dilution in the CO_2-rich phase, equation (3-21) reduces to the following relation for H_2O:

$$\ln \emptyset_i = \ln\left(\frac{v_{CO_2}}{v_{CO_2} - b_{mix}}\right) + \frac{b_i}{v_{CO_2} - b_{mix}} - \frac{2a_{H_2O-CO_2}}{b_{mix} RT^{3/2}} \ln\left(\frac{v_{CO_2} + b_{mix}}{v_{CO_2}}\right) + \frac{a_{mix} b_i}{b_{mix}^2 RT^{3/2}} \left[\ln\left(\frac{v_{CO_2} + b_{mix}}{v_{CO_2}}\right) - \frac{b_{mix}}{v_{CO_2} + b_{mix}}\right] - \ln Z_{CO_2} \quad \text{3- 25}$$

Fitted Redlich-Kwong parameters by N. Spycher, K. Pruess and Ennis-King [59, 85] are given in table 3. Values of b_{H_2O} and $a_{H_2O-CO_2}$ were derived assuming infinite dilution of H_2O in the compressed gas phase (i.e. $y_{H_2O} = 0$ *and* $y_{CO_2} = 1$ in the mixture). The uncertainty represents 95% confidence. The fitted *T* range is 283-380 K.

Table 3 shows the coefficients values for Redlich-Kwong equation.

Parameter	Value	Units
a_{CO_2}	$7.54 \times 10^7 - 4.13 \times 10^4 \times T(K)$	$bar\ cm^6\ K^{0.5}\ mol^{-2}$
b_{CO_2}	27.80 ($\pm$0.01)	cm^3/mol
b_{H_2O}	18.18 ($\pm$1.05)	cm^3/mol
$a_{H_2O-CO_2}$	6.23×10^7 ($\pm 0.08 \times 10^7$)	$bar\ cm^6\ K^{0.5}\ mol^{-2}$

However, under the hypothesis of infinite H_2O dilution in the CO_2-rich phase, a_{mix} and b_{mix} parameters are equal to *a* and *b* parameters of pure CO_2.

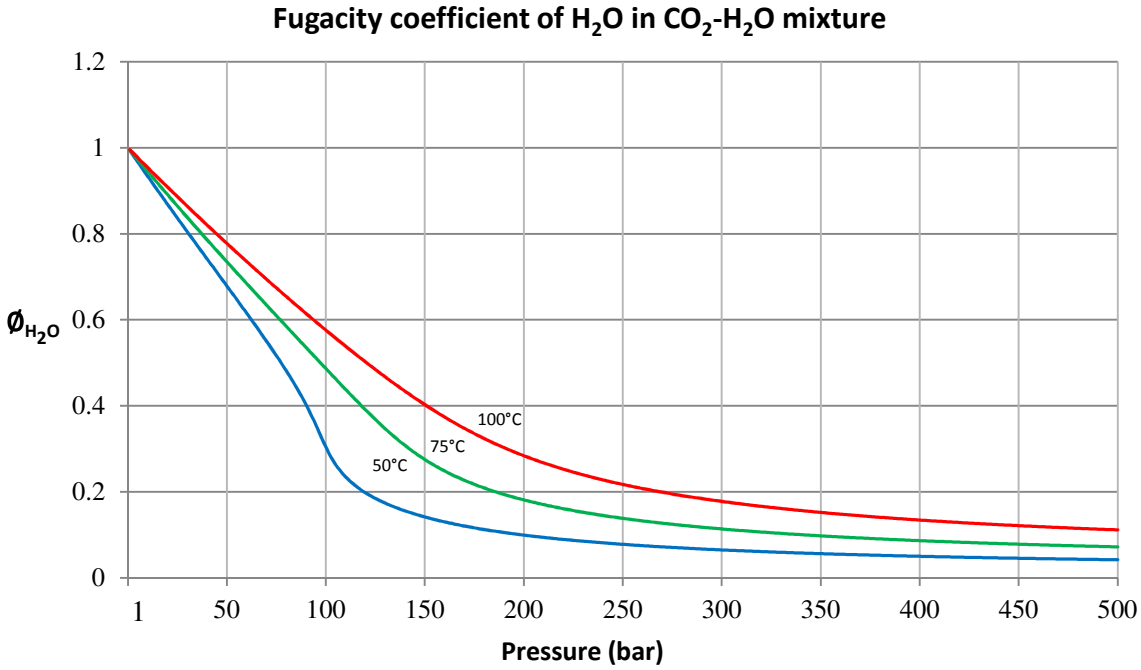

Figure 7. Fugacity coefficient of H_2O computed at 50, 75 and 100°C and variable pressures by means of the Redlich-kwong equation.

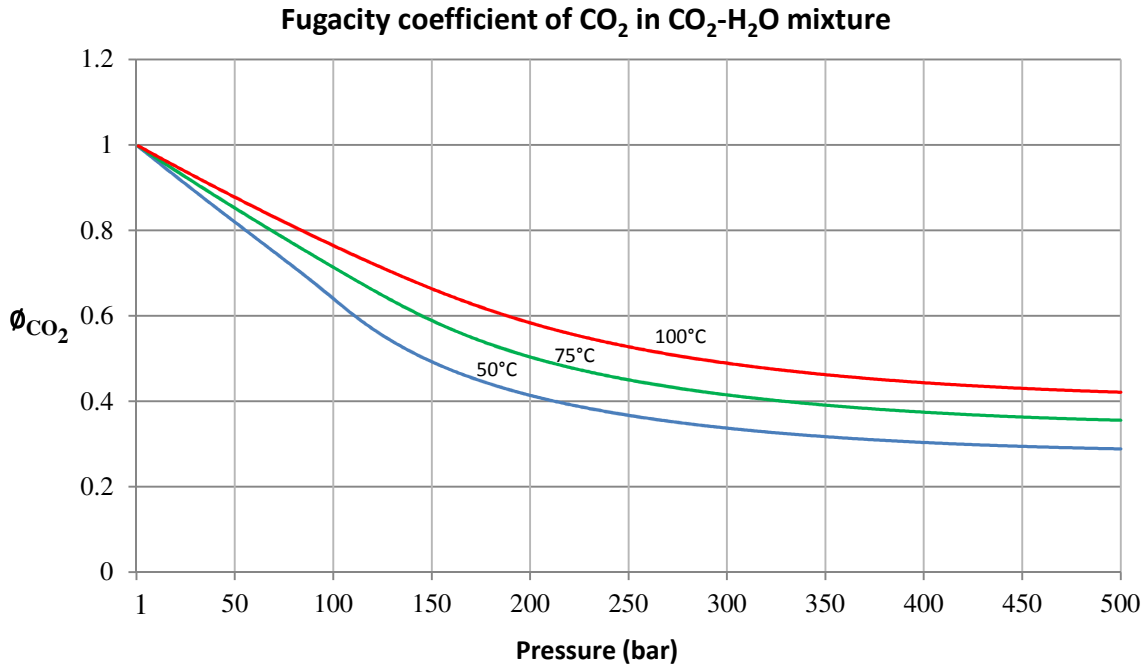

Figure 8. Fugacity coefficient of CO_2 computed at 50, 75 and 100°C and variable pressures by means of the Redlich-kwong equation.

Figure 7 and 8 depict the variation of fugacity coefficient of carbon dioxide and water with the pressure in reservoir conditions (a temperature range of 50 to 100°C and pressure up to 500 bar).The fugacity coefficient of CO_2 is generally higher than that of H_2O. However, both of them exhibit similar behavior with regard to variations in pressure. Fugacity coefficients decrease with increase in pressure. At higher temperatures, the respective fugacity coefficients are found to be higher than values at lower temperature. The fugacity coefficients of CO_2 in CO_2-H_2O mixtures are used to calculate the solubility of CO_2 in the mixtures. According to the thermodynamics equilibrium constants at given *T*, *P*, the solubility of carbon dioxide increases as the fugacity increases.

3.9. Mutual solubility of CO_2 and H_2O in CO_2-H_2O mixtures

Thermodynamics equilibrium constants at any given *T*, *P* are:

$$H_2O_{(l)} \Leftrightarrow H_2O_{(g)} \quad \rightarrow \quad K_{H_2O,T,P} = \frac{a_{H_2O_{(g)}}}{a_{H_2O_{(l)}}} = \frac{f_{H_2O_{(g)}}/f^{\circ}_{H_2O_{(g)}}}{a_{H_2O_{(l)}}} \qquad 3\text{-}26$$

$$CO_{2(aq)} \Leftrightarrow CO_{2(g)} \quad \rightarrow \quad K_{CO_2,T,P} = \frac{a_{CO_{2(g)}}}{a_{CO_{2(aq)}}} = \frac{f_{CO_{2(g)}}/f^{\circ}_{CO_{2(g)}}}{a_{CO_{2(aq)}}} \qquad 3\text{-}27$$

The mole fraction of dissolved CO_2 is related to its molal concentration:

$$x_{CO_2} = \frac{m_{CO_2}}{m_{CO_2} + m_{H_2O}} = \frac{m_{CO_2}}{m_{CO_2} + \frac{1000}{18.02}} \rightarrow \quad m_{CO_2} = \frac{x_{CO_2} \times 55.5}{(1 - x_{CO_2})} \cong x_{CO_2} \times 55.5 \qquad 3\text{-}28$$

By taking the activity coefficient of dissolved CO_2, γ_{CO2} equal to 1:

$$a_{CO_2} = m_{CO_2}\, \gamma_{CO_2} \cong x_{CO_2} \times 55.5 \qquad 3\text{-}29$$

Therefore:

$$K_{H_2O,T,P} = \frac{a_{H_2O_{(g)}}}{a_{H_2O_{(l)}}} = \frac{f_{H_2O_{(g)}}/f^{\circ}_{H_2O_{(g)}}}{a_{H_2O_{(l)}}} \cong \frac{f_{H_2O_{(g)}}}{1 - x_{CO_2}} \qquad 3\text{-}30$$

$$K_{CO_2,T,P} = \frac{a_{CO_{2(g)}}}{a_{CO_{2(aq)}}} = \frac{f_{CO_{2(g)}}/f^{\circ}_{CO_{2(g)}}}{a_{CO_{2(aq)}}} = \frac{f_{CO_{2(g)}}}{x_{CO_2} \times 55.5} \qquad 3\text{-}31$$

The temperature dependence of these equilibrium constants are (T in ℃):

$$log\, K_{H_2O,T,P^{\circ}} = -2.209 + 0.03097\, T - 0.0001098\, T^2 + 2.048 \times 10^{-7}\, T^3 \qquad 3\text{-}32$$

$$\log K_{CO_2(g),T,P^{\circ}} = 1.189 + 0.01304\, T - 5.446 \times 10^{-5}\, T^2 \qquad 3\text{-}33$$

$$\log K_{CO_2(l),T,P^{\circ}} = 1.169 + 0.01368\, T - 5.380 \times 10^{-5}\, T^2 \qquad 3\text{-}34$$

The respective values for the equilibrium constants at different temperatures are given in Table 4.

Table 4. shows the equilibrium constants values at 50, 75 and 100°C.

Temperature (T in °C)	50°C	75°C	100°C
K_{H_2O,T,P°	0.123197	0.382406	0.988098
$K_{CO_2(l),T,P^\circ}$	52.2998	78.0504	88.77

In these calculations $K_{CO_2(g),T,P^\circ}$ is used when the temperature and the volume of the gas phase are above the critical parameters of CO_2, 31°C and 94 $cm^3\ mol^{-1}$. $K_{CO_2(l),T,P^\circ}$ is used when the temperature and the volume of the gas phase are below the critical parameters of CO_2.

Whereas the effect of pressure is taken into account:

$$K_{T,P} = K_{T,P^\circ}\ exp\left(\frac{\left(P - P^\circ\right)\bar{V}_i}{RT}\right) \qquad 3\text{- }35$$

here, $\bar{V}_i$ is the average molar volume.

where, $P^\circ = 1\ bar$ and $\bar{V}_{H_2O} = 18.1\ cm^3\ mol^{-1}$, $\bar{V}_{CO_2} = 32.6\ cm^3\ mol^{-1}$.

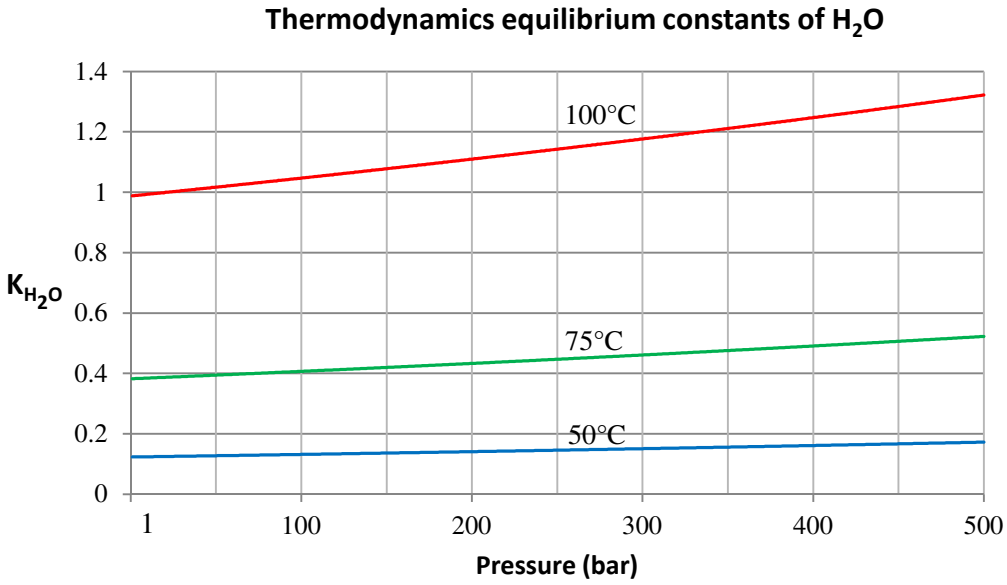

Figure 9. Thermodynamics equilibrium constants of H_2O computed at 50, 75 and 100°C and variable pressures by means of the Redlich-kwong equation.

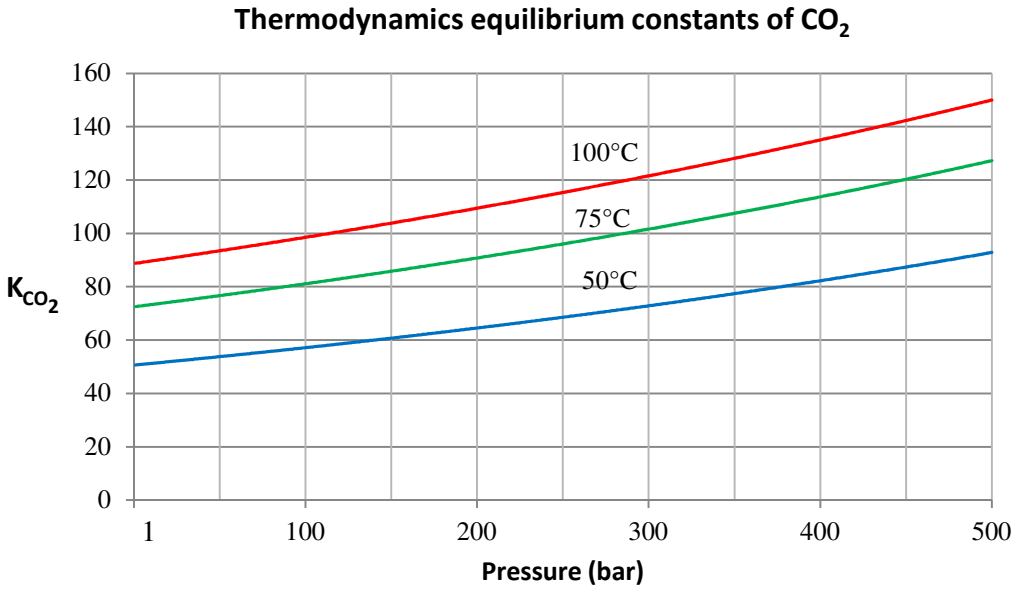

Figure 10. Thermodynamics equilibrium constants of CO_2 computed at 50, 75 and 100°C and variable pressures by means of the Redlich-kwong equation.

Figure 9 and 10 depict the variation of thermodynamics equilibrium constants of carbon dioxide and water with the pressure in reservoir conditions (a temperature range of 50 to 100°C and pressure up to 500 bar). It is seen the thermodynamic equilibrium constants increase proportionately with both increase in pressure and temperature.

3.10. The activity coefficient of CO_2 in NaCl solutions

According to Helgeson for computing the activity coefficient of $CO_{2(aq)}$ in NaCl solutions of different molalities based on the Henry's law coefficients of Ellis and Golding [86, 87]:

$$CO_{2(aq)} \rightleftharpoons CO_{2(g)} \qquad 3\text{- }36$$

$$K_{CO_2} = \frac{a_{CO_2(g)}}{a_{CO_2(aq)}} = \frac{f_{co_{2(g)}}/f^{\circ}_{co_2(g)}}{m_{CO_2(g)} \times \gamma_{CO_2(aq)}} \qquad 3\text{- }37$$

Since pH of the system after dissolution of CO_2 is less than 6.3, it is safe to assume that concentration of H_2CO_3 dominates the total concentration. In other words, concentrations of HCO_3^- and CO_3^{2-} can be neglected. The activity coefficient of CO_2 can be determined

experimentally. This approach followed by Helgeson to compute the activity coefficient of CO_2 in NaCl solutions of different molalities based on the Henry's law coefficients of Ellis and Golding [86]:

$$\gamma_{CO_2} = \frac{f_{co_{2(g)}}}{m_{CO_2(g)} \times K_{CO_2}} = \frac{K_{H,CO_2,sol}}{K_{H,CO_2,water}} \quad 3\text{-}38$$

where, $K_{H,CO_2,sol}$ and $K_{H,CO_2,water}$ are respectively the Henry's Law coefficients for the saline solution and for pure water as solvent [86]. The most applicable has been expressed by Ellis and Golding, who used solubility data to calculate Henry's law coefficients, K_H, for carbon dioxide in water and NaCl solutions [86, 87]:

$$k = \frac{1}{m} \log\left(\frac{K_H}{K_H^{\circ}}\right) \quad 3\text{-}39$$

here, *k* is the salting-out coefficient, *m* is the molality of NaCl, and K_H° and K_H are respectively the Henry's law coefficients for pure water as solvent and for the saline solution [86]. Adding salt to the system CO_2-H_2O increases the Henry's law coefficient and decreases the solubility of carbon dioxide in the solution. Activity coefficient for CO_2 can be expressed by the following equation:

$$\gamma_{CO_2} = 10^{k \times m} \quad 3\text{-}40$$

here, *k* is the salting-out coefficient, *m* is the molality of *NaCl*. Salting-out coefficient is temperature dependent and can be determined by following equation [86]:

$$k = a + bT + cT^2 + dT^3 + e \log T \quad 3\text{-}41$$

Coefficients for use equation (3-41) are given in Table 5 [63].

Table 5. shows the coefficients values which are used in equation (3-41).

	a	b	c	d	e
k	108.875	0.174114604	$-1.9845113 \times 10^{-4}$	1.0131668×10^{-7}	-58.867703

At a given temperature salting-out coefficient can be calculated, by knowing the molality of NaCl, the ratio of Henry's law coefficients can be determined which is equal to activity coefficients of CO_2 in NaCl solutions. The Henry's law coefficient at given temperature can be calculated by following equation:

$$K_H = -7656970 - 3122.11449\,T + 1.092229\,T^2 + 1.880778 \times 10^8\,T^{-1} + 3.1771246 \times 10^6\,\log T \quad \text{3- 42}$$

In this study, the activity coefficients of CO_2 are calculated based on the fugacity of CO_2 calculated through the corresponding values of molar volume and thermodynamic equilibrium constants**:**

$$\gamma_{CO_2} = \frac{f_{co_{2(g)}}}{m_{CO_{2(g)}} \times K_{CO_2}} \quad \text{3- 43}$$

Activity coefficients of dissolved CO_2 from Helgeson's experimental results are given in Table 6.

Table 6. Shows activity of water and activity coefficient of dissolved CO_2 for 1, 2 and 3 mol kg^{-1} NaCl aqueous solutions (from Helgeson, 1969) at the temperatures of interest (values at 75°C have been obtained by interpolation).

m_{NaCl}	Temperature			
	25℃	50℃	75℃	100℃
Activity of water $\left(a_{H_2O_{(l)}}\right)$				
1	0.9669	0.9667	0.9667	0.9669
2	0.9316	0.9308	0.9308	0.9315
3	0.8932	0.8919	0.8918	0.893
Activity coefficient of dissolved $CO_2\left(\gamma_{CO_2}\right)$				
1	1.27	1.24	1.22	1.20
2	1.57	1.50	1.46	1.44
3	1.93	1.80	1.75	1.74

Figure 11 depicts the variation of activity coefficient of carbon dioxide with variable temperature in reservoir conditions (a temperature range of 25 to 100˚C). The model calculates the acitivity coefficient with respect to the molar volume of supercritical CO_2. It has been found to be in good agreement with Helgeson's experimental results in supercritical range (a temperature range of 50 to 100˚C).

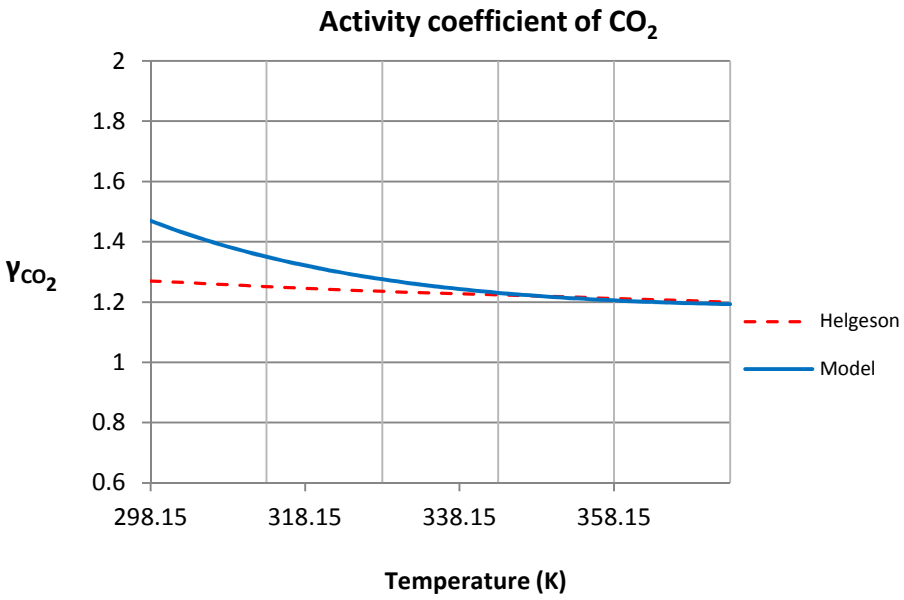

Figure 11. Activity coefficient of CO_2 computed at 1 bar and variable temperatures by means of the Redlich-kwong equation.

3.11. Mole fraction of CO_2 in liquid phase

According to the previous equation:

$$f_i = \varphi_i \, y_i \, P \qquad 3\text{- }44$$

here, y_i denotes the mole fraction of the *i*th component in the gas mixture.

$$f_{H_2O_{(g)}} = \varphi_{H_2O} \times y_{H_2O} \times P = K_{H_2O,T,P} \times \left(1 - x_{CO_2}\right) \qquad 3\text{- }45$$

$$f_{CO_{2(g)}} = \varphi_{CO_2} \times y_{CO_2} \times P = K_{CO_2,T,P} \times x_{CO_2} \times 55.5 \qquad 3\text{- }46$$

$$y_{H_2O} = \frac{K_{H_2O,T,P^\circ}\left(1 - x_{CO_2}\right)}{\varphi_{H_2O} \times P} exp\left(\frac{\left(P - P^\circ\right) \times 18.1}{RT}\right) \qquad 3\text{- }47$$

$$x_{CO_2} = \frac{\varphi_{CO_2} \times y_{CO_2} \times P}{K_{CO_2,T,P^\circ} \times 55.5} exp\left(-\frac{\left(P - P^\circ\right) \times 32.6}{RT}\right)$$

$$= \frac{\varphi_{CO_2} \times \left(1 - y_{H_2O}\right) \times P}{K_{CO_2,T,P^\circ} \times 55.5} exp\left(-\frac{\left(P - P^\circ\right) \times 32.6}{RT}\right) \quad \text{3- 48}$$

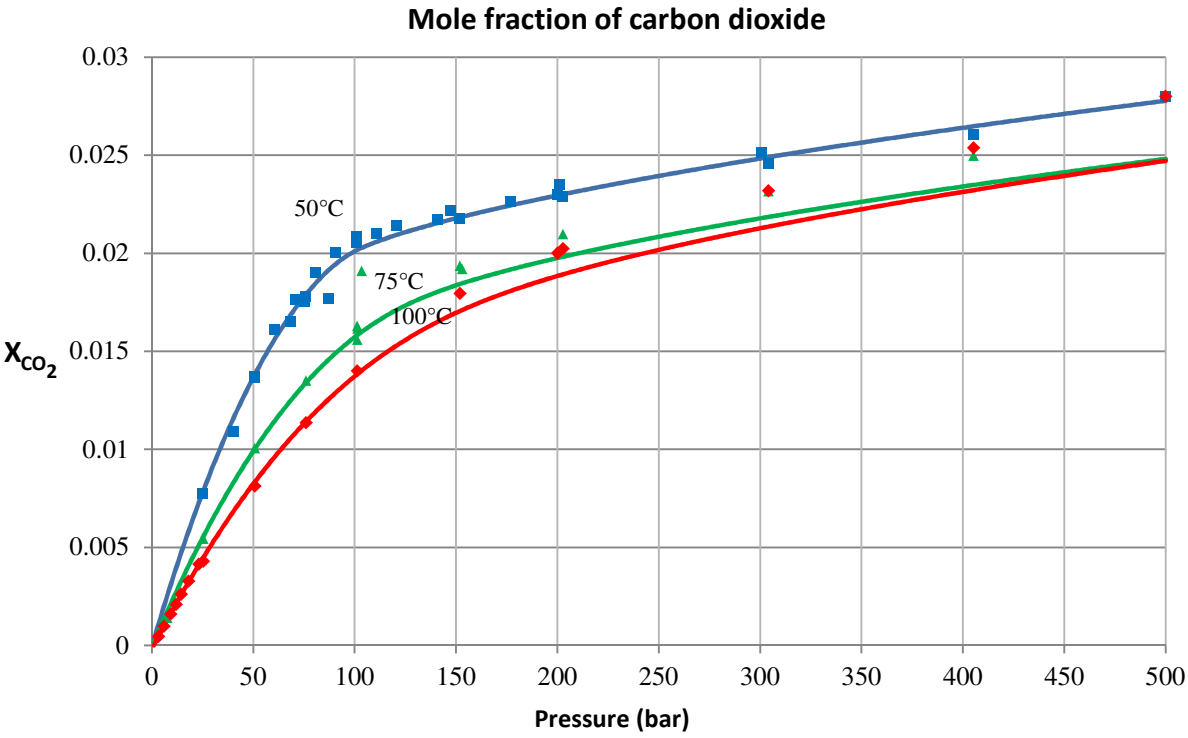

Figure 12. Mole fraction of CO_2 in aqueous phase verses pressure at various temperatures: Comparison of model results (lines) with Nicolas Spycher and Karsten Pruess' experimental data (symbols) (2003).

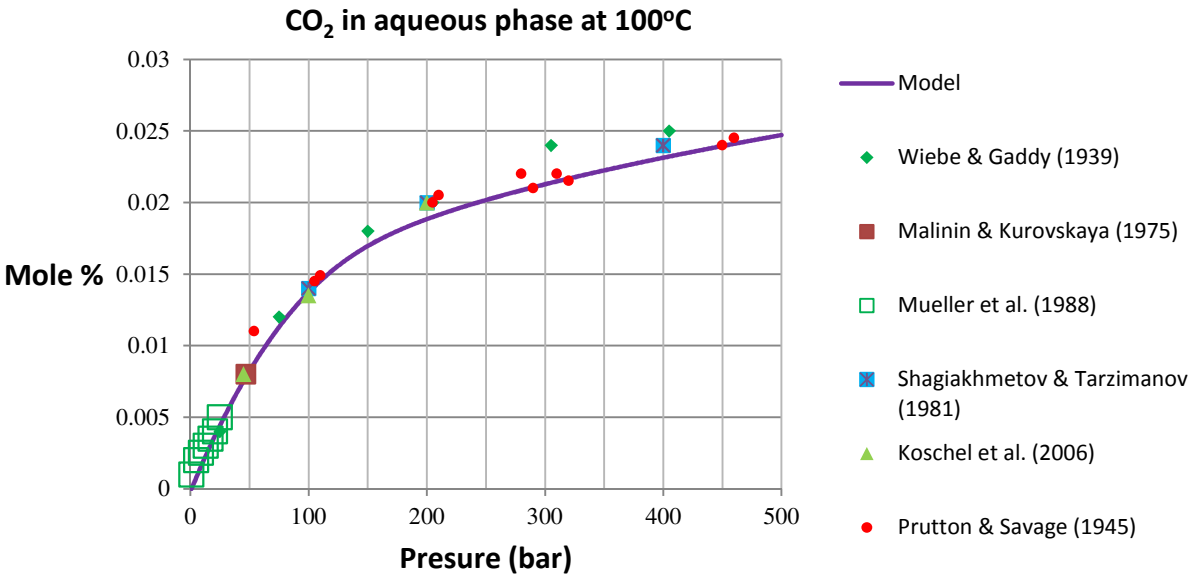

Figure 13. Mutual solubility of CO_2 and pure water: Comparison of model results (line) with experimental data (symbols) at 100°C and up to 500 bar.

The mole fraction of CO_2 in aqueous phase without salinity has been found to increase with increase in pressure. However temperature has an adverse effect on the mole fraction. Higher temperatures lead to decreasing mole fractions. According to the Figure 12 and Figure 13, for the most part, mutual solubilities of CO_2 in liquid phase reported from the other researchers are in good agreement with the results in this method but in figure 12 there is discrepancy between model and experimental data at higher temperatures and pressures. Differences between experimental and calculated results is due to the hypothesis of infinite dilution of water in CO_2-rich liquid phase [13] and also may arise due to factors not accounted for in the theoretical model including, i.e. aquifer heterogeneity, diffusion and convection. The average of the deviations from the model line was found using the available data points from experiments and is given in Table 7.

Table 7 shows the average deviations (in percent) of experimental results from the model.

Previous experimental results	Average deviation (%)
Wiebe & Gaddy(1939)	7.24
Malinin & Kurovskaya(1975)	2.32
Muller et al.(1988)	9.74
Shagiakhmetov & Tarzimanov(1981)	3.97
Koschel et al.	3.25
Prutton & Savage	4.89

This approach can be used for calculating mutual solubilities of CO_2 and H_2O in CO_2-H_2O mixtures compare with experimental data. Peng-Robinson EOS is also applied to compute the solubility of CO_2-H_2O mixtures from 25 to 350°C and up to 1,000 bar. The Peng-Robinson EOS is more complex than the Redlich-Kwong equation, and it reproduces the liquid-vapor boundary with good accuracy [88].

3.12. Impact of dissolved salts on the mutual solubility of CO_2 and H_2O

The previous equation should be modified by changing the activity of liquid water and the activity coefficient of dissolved CO_2, which was assumed to be unity for the CO_2-H_2O binary.

$$y_{H_2O} = \frac{K_{H_2O,T,P^\circ}\ a_{H_2O}}{\varphi_{H_2O} \times P} exp\left(\frac{\left(P - P^\circ\right) \times 18.1}{RT}\right) \quad 3\text{-}49$$

At this point, the mole fraction of CO_2 in the aqueous phase is:

$$x_{CO_2} = \frac{m_{CO_2}}{m_{CO_2} + m_{H_2O} + 2 \times m_{NaCl}} = \frac{m_{CO_2}}{m_{CO_2} + 55.508 + 2 \times m_{NaCl}} \quad 3\text{-}50$$

$$m_{CO_2} = \frac{x_{CO_2}\ (55.508 + 2 \times m_{NaCl})}{1 - x_{CO_2}} \quad 3\text{-}51$$

For this system, since we assume complete dissociation of dissolved NaCl into Na^+ and Cl^- ions:

$$a_{CO_2} = m_{CO_2}\,\gamma_{CO_2} = \frac{x_{CO_2}\,(55.508 + 2 \times m_{NaCl})}{1 - x_{CO_2}}\,\gamma_{CO_2} \qquad 3\text{- }52$$

According to previous equations:

$$K_{CO_2,T,P} = \frac{a_{CO_{2(g)}}}{a_{CO_{2(aq)}}} = \frac{f_{CO_{2(g)}}/f^{\circ}_{CO_{2(g)}}}{a_{CO_{2(aq)}}} = \frac{f_{CO_{2(g)}}}{a_{CO_{2(aq)}}} \qquad 3\text{- }53$$

$$a_{CO_{2(aq)}} = \frac{f_{CO_{2(g)}}}{K_{CO_2,T,P}} = \frac{\varphi_{CO_2} \times y_{CO_2} \times P}{K_{CO_2,T,P^\circ}\ exp\left(\frac{(P - P^\circ) \times 32.6}{RT}\right)} = \frac{\varphi_{CO_2} \times (1 - y_{H_2O}) \times P}{K_{CO_2,T,P^\circ}}\ exp\left(-\frac{(P - P^\circ) \times 32.6}{RT}\right) \qquad 3\text{- }54$$

By solving two equations, $a_{CO_{2(aq)}}$ and x_{CO_2} can be calculated.

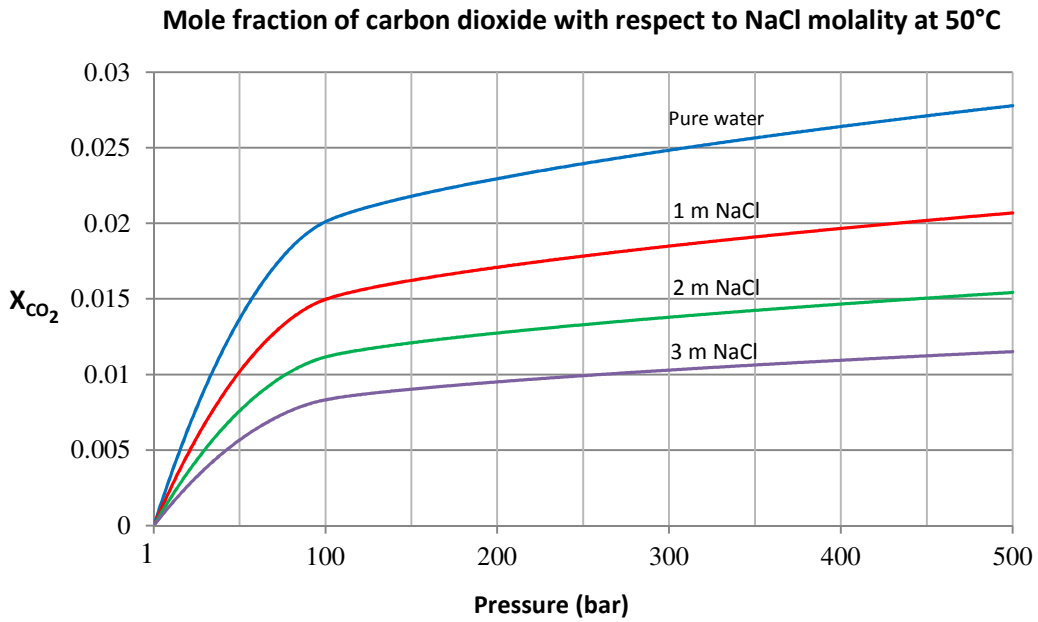

Figure 14. Mole fraction of CO_2 in pure and saline water computed at 50°C and variable pressures and salinity by means of the Redlich-kwong equation.

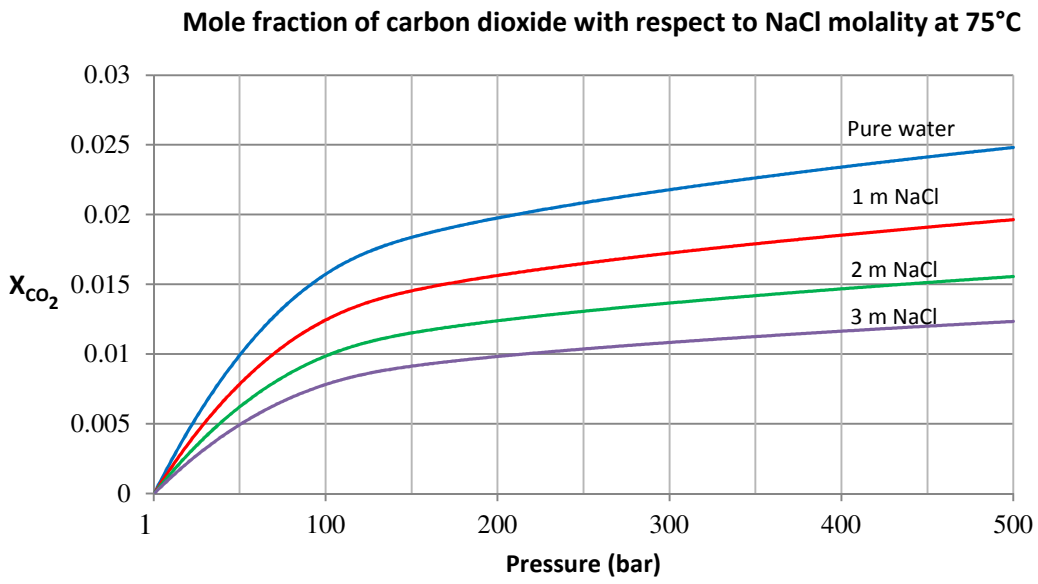

Figure 15. Mole fraction of CO_2 in pure and saline water computed at 75°C and variable pressures and salinity by means of the Redlich-kwong equation.

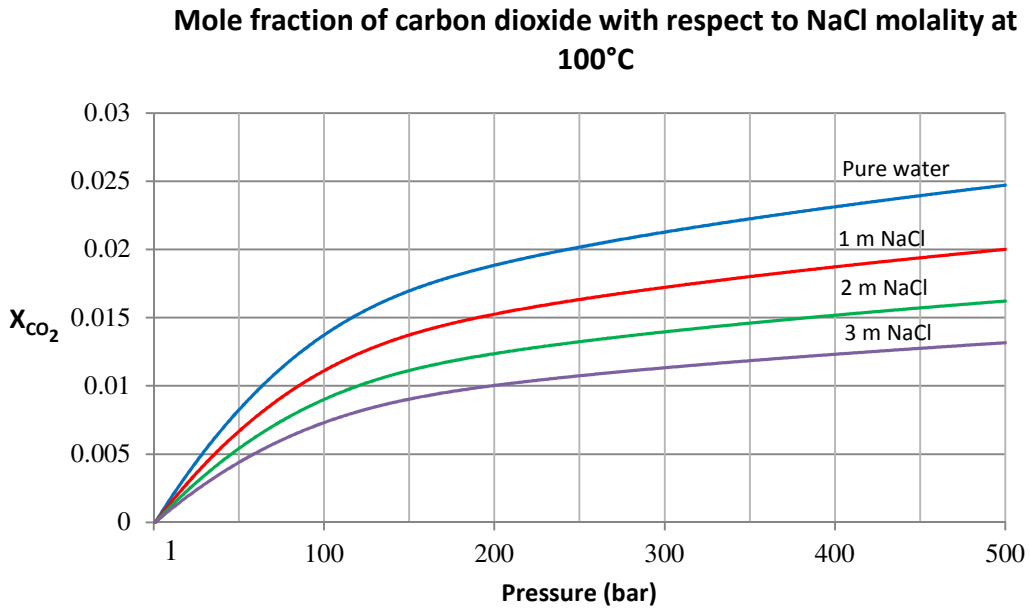

Figure 16. Mole fraction of CO_2 in pure and saline water computed at 100°C and variable pressures and salinity by means of the Redlich-kwong equation.

As can be observed in figure 14, 15 and 16 the mole fraction of CO_2 increases as the pressure increases. However, the mole fraction of CO_2 decreases as the molality of NaCl increases.

3.13. pH of the system after dissolution of CO_2 in brine

After dissolution of CO_2 in brine, carbon dioxide exists in equilibrium with carbonic acid:

$$CO_2 + H_2O \rightleftharpoons H_2CO_3 \quad \text{3- 55}$$

The hydration equilibrium constant at 25 °C is called K_h, which in the case of carbonic acid is $[H_2CO_3]/[CO_2] = 1.70\times10^{-3}$: hence, the majority of the carbon dioxide is not converted into carbonic acid, remaining as CO_2 molecules. [18, 19] Carbonic acid is diprotic; it has two protons, which may dissociate from the parent molecule. Thus there are two dissociation constants, the first one for the dissociation into the bicarbonate (also called hydrogen carbonate) ion: [20, 21]

$$H_2CO_3 \rightleftharpoons HCO_3^- + H^+ \quad \rightarrow \quad K_{a1} = 4.45 \times 10^{-7} \quad \rightarrow \quad pK_{a1} = 6.352 \; at \; 25℃ \quad \text{3- 56}$$

The second for the dissociation of the bicarbonate ion into the carbonate ion CO_3^{2-}:

$$HCO_3^- \rightleftharpoons CO_3^{2-} + H^+ \quad \text{3- 57}$$

$$K_{a2} = 4.69 \times 10^{-11} \quad \rightarrow \quad pK_{a2} = 10.329 \text{ at } 25℃ \text{ and Ionic strength} = 0.0 \quad \text{3- 58}$$

Concentration of $[H^+]$ can be expressed by: [19, 20]

$$[H^+] \approx \left(10^{-14} + \frac{K_h K_{a1} f_{CO_{2(g)}}}{K_H}\right)^{1/2} \quad \text{3- 59}$$

According to this equation, concentration of H^+ can be determined at given temperature and pressure. Henry's coefficient is also temperature dependent. Therefore concentration of H^+ can be affected by variation of pressure and temperature. According to the previous equation, concentration of H^+ increases as pressure increases. Accordingly, pH of the system can be calculated based on concentration of H^+ by the following equation:

$$pH = -log[H^+] \quad \text{3- 60}$$

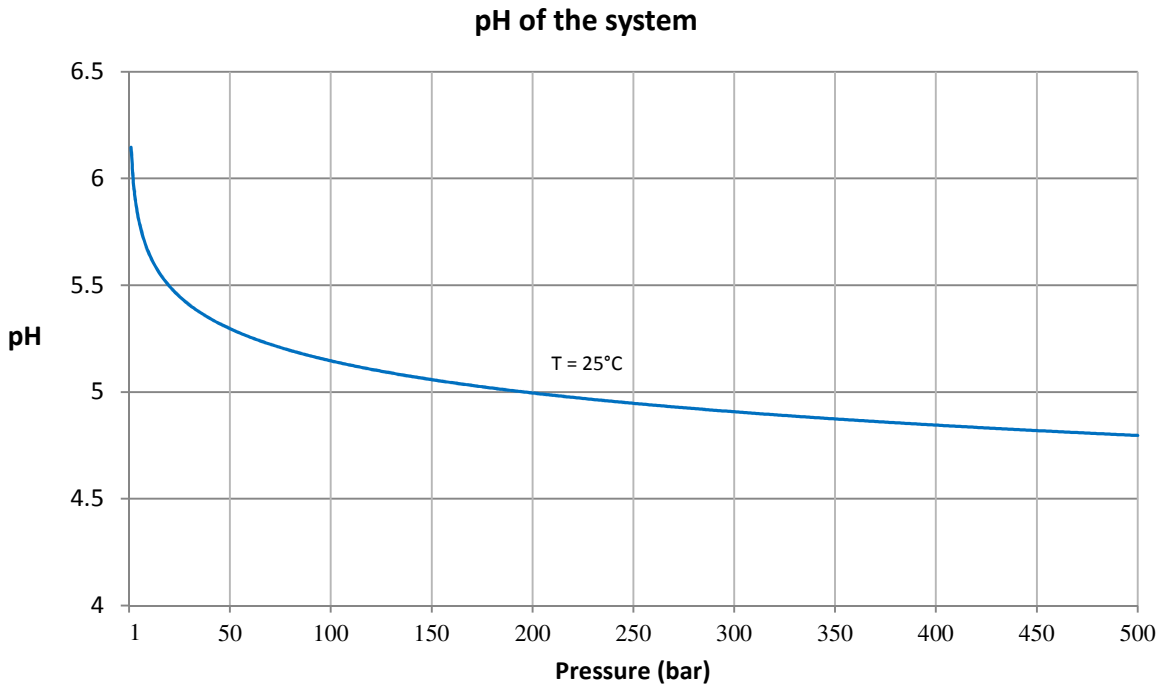

Figure 17. pH of the system computed at 25, 50, 75 and 100°C and variable pressures.

Figure 17 depicts the variation of pH with respect to the change in pressure. The pH decreases with an increase of the pressure of the system. In other words, the greater the pressure above the brine the more acidic is the brine. Due to the carbonic acid, pH of the system decreases after dissolution of CO_2. Carbon dioxide is soluble in water, in which it spontaneously interconverts between CO_2 and H_2CO_3 (carbonic acid). The relative concentrations of CO_2, H_2CO_3, and the deprotonated forms HCO_3^- (bicarbonate) and CO_3^{2-}(carbonate) depend on the concentration of H^+:

$$H_2O(l) + CO_2(g) \rightarrow H_2CO_3(aq) \qquad \log K = -1.46 \qquad 3\text{- }61$$

$$H_2CO_3(aq) \rightarrow HCO_3^-(aq) + H^+(aq) \qquad \log K = -6.35 \qquad 3\text{- }62$$

$$HCO_3^-(aq) \rightarrow CO_3^{2-}(aq) + H^+(aq) \qquad \log K = -10.33 \qquad 3\text{- }63$$

$$H_2O \rightarrow H^+(aq) + OH^-(aq) \qquad \log K = -14 \qquad 3\text{- }64$$

Distribution of aqueous species in an open system without salinity, so the activity coefficients are 1: [7]

$$[H_2CO_3] = K_H P_{CO_2} \qquad 3\text{- }65$$

$$K_{a1} = \frac{[HCO_3^-][H^+]}{[H_2CO_3]} \quad \rightarrow \quad [HCO_3^-] = \frac{K_{a1}[H_2CO_3]}{[H^+]} = \frac{K_{a1}K_H P_{CO_2}}{[H^+]} \qquad 3\text{- }66$$

$$K_{a2} = \frac{[CO_3^{2-}][H^+]}{[HCO_3^-]} \quad O - \ [CO_3^{2-}] = \frac{K_{a2}[HCO_3^-]}{[H^+]} = \frac{K_{a2}K_{a1}K_H P_{CO_2}}{[H^+]^2} \qquad 3\text{- }67$$

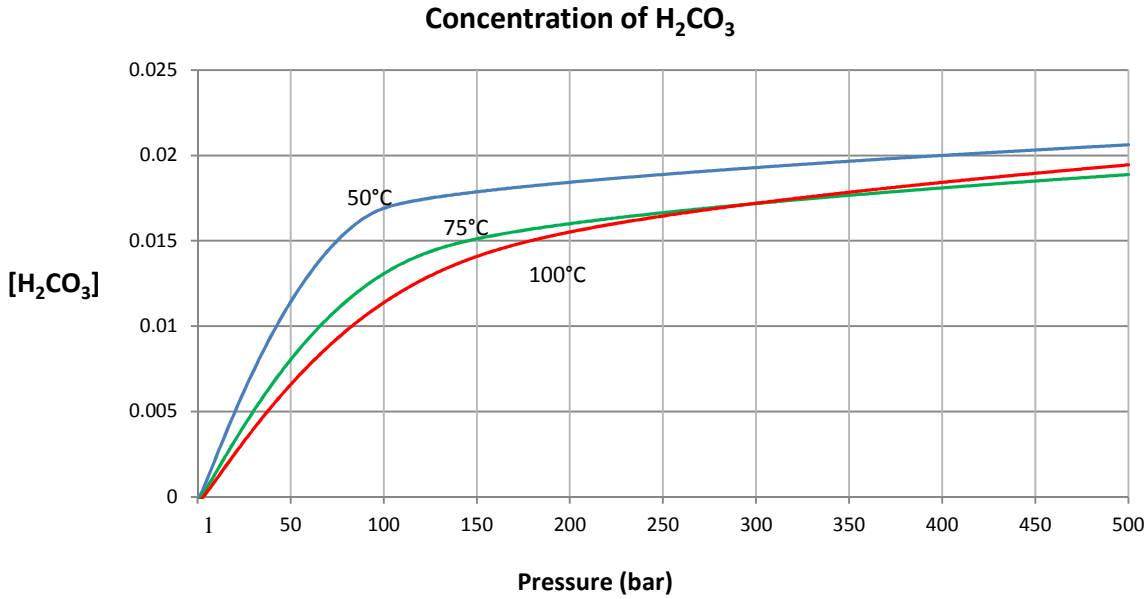

Figure 18. Concentration of H_2CO_3 computed at 50, 75 and 100°C and variable pressures.

As could be seen in figure 18, concentration of H_2CO_3 increases as the pressure increases. But temperature has an adverse effect on concentration of H_2CO_3. In other words, the higher temperatures lead to decreasing the concentration of H_2CO_3 at lower pressure.

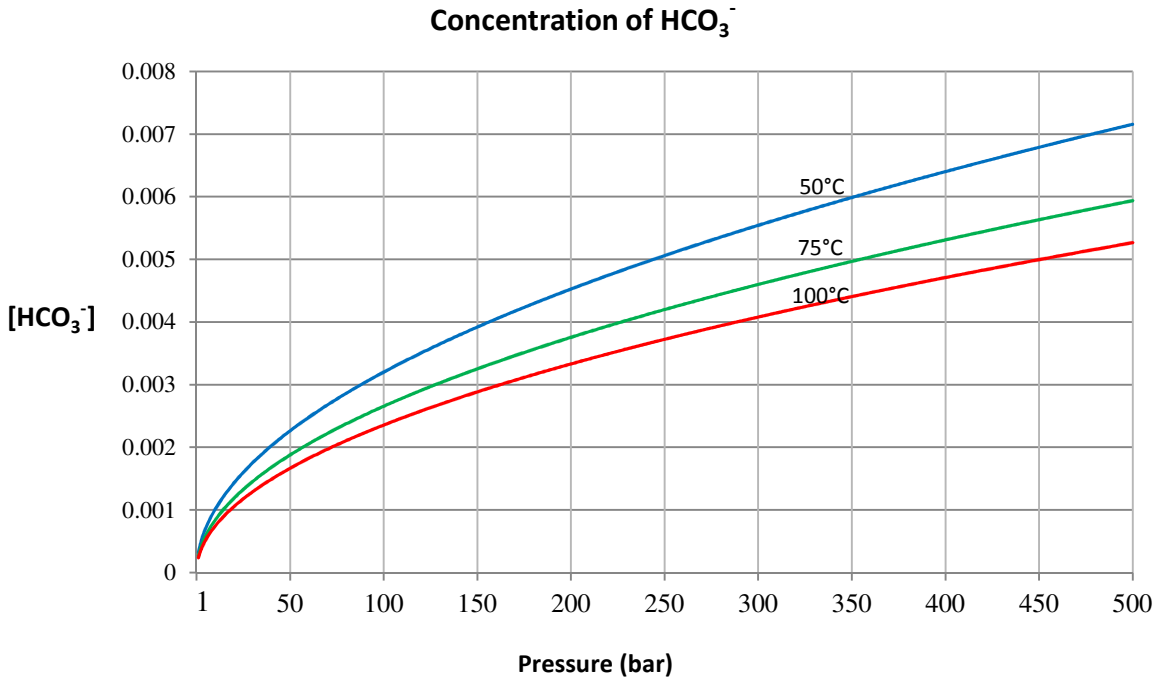

Figure 19. Concentration of HCO_3^- computed at 50, 75 and 100°C and variable pressures.

It is indicated in figure 19, concentration of HCO_3^- increases with increase in pressure. However, increase in temperature will result in decrease of concentration.

Concentration of CO_3^{2-} remains very small. In other words, based on the pH of the system, concentration of H_2CO_3 dominates the total concentration.

3.14. Conclusion

In the above-mentioned text the equations needed to carry out thermodynamic equilibrium calculations between liquids and gases have been recalled. This chapter is focused on CO_2-H_2O fluids. It has been found that, the greater the pressure above the brine the more soluble CO_2 is in the brine. In other words, the mole fraction of CO_2 increases as the pressure increases. However, temperature and salinity have inverse effects on solubility of CO_2 in aqueous phase. Therefore, higher temperatures and salinities lead to decreasing solubility of CO_2. For the moment aquifer rocks have been assumed are totally unreactive in the short-term behavior of our system. Furthermore, the reactions between fluids and aquifer rocks should be taken into account to predict the long-term behavior of the system. Next chapter is devoted to briefly review the

structure of calcite and the thermodynamic stability of the other expected product solid phases of geological CO_2 sequestration and mineral carbonation.

Chapter 4: Major carbonate minerals

4.1. The stability of the carbonate minerals of Ca and Mg

Virtually permanent CO_2 sequestration in form of solid carbonates into relatively deep geological formations is one approach to get a rid of large amounts of CO_2. This approach involves the dissolution of primary phases and the precipitation of new phases, mainly carbonates. Calcite is the most important carbonate minerals and has been the subject of several geochemical investigations recently [89, 90]. Since the thermodynamic properties of Ca-, Mg- minerals are known; let us investigate their stabilities in the system. For example, in deep reservoirs conditions, fugacity values of CO_2 are high, so calcite is a wide spread mineral. On the other hand, Portlandite exists at low fugacity values of CO_2 that rarely can be found in deep reservoirs conditions.

Table 8. shows thermodynamic equilibrium constants:

$Ca(OH)_{2(s)} + Mg^{2+} \rightleftharpoons Mg(OH)_{2(s)} + Ca^{2+}$	$\log\left(\frac{a_{Ca^{2+}}}{a_{Mg^{2+}}}\right) = \log K = 6.2572$
$CaCO_{3(s)} + Mg^{2+} + H_2O \rightleftharpoons Mg(OH)_{2(s)} + Ca^{2+} + CO_{2(g)}$	$\log\left(\frac{a_{Ca^{2+}}}{a_{Mg^{2+}}}\right) = -6.6357 - \log f_{CO_2}$
$CaMg(CO_3)_{2(s)} + Mg^{2+} + 2H_2O \rightleftharpoons 2Mg(OH)_{2(s)} + Ca^{2+} + 2CO_{2(g)}$	$\log\left(\frac{a_{Ca^{2+}}}{a_{Mg^{2+}}}\right) = -14.45 - 2 \cdot \log f_{CO_2}$
$2CaCO_{3(s)} + Mg^{2+} \rightleftharpoons CaMg(CO_3)_{2(s)} + Ca^{2+}$	$\log\left(\frac{a_{Ca^{2+}}}{a_{Mg^{2+}}}\right) = \log K = 1.1839$
$CaMg(CO_3)_{2(s)} + Mg^{2+} \rightleftharpoons 2MgCO_{3(s)} + Ca^{2+}$	$\log\left(\frac{a_{Ca^{2+}}}{a_{Mg^{2+}}}\right) = \log K = -2.0737$
$CaMg_3(CO_3)_{4(s)} + Mg^{2+} + 4H_2O \rightleftharpoons 4Mg(OH)_{2(s)} + Ca^{2+} + 4CO_{2(g)}$	$\log\left(\frac{a_{Ca^{2+}}}{a_{Mg^{2+}}}\right) = -23.64 - 4 \cdot \log f_{CO_2}$
$\frac{4}{3}CaCO_{3(s)} + Mg^{2+} \rightleftharpoons \frac{1}{3}CaMg_3(CO_3)_{4(s)} + Ca^{2+}$	$\log\left(\frac{a_{Ca^{2+}}}{a_{Mg^{2+}}}\right) = \log K = -0.9687$

$2CaMg(CO_3)_{2(s)} + Mg^{2+} \rightleftharpoons CaMg_3(CO_3)_{4(s)} + Ca^{2+}$	$\log\left(\frac{a_{Ca^{2+}}}{a_{Mg^{2+}}}\right) = \log K = -5.2740$
$CaMg_3(CO_3)_{4(s)} + Mg^{2+} \rightleftharpoons 4MgCO_{3(s)} + Ca^{2+}$	$\log\left(\frac{a_{Ca^{2+}}}{a_{Mg^{2+}}}\right) = \log K = 1.1266$
$CaMg(CO_3)_{2(s)} + Mg^{2+} + 2H_2O \rightleftharpoons 2Mg(OH)_{2(s)} + Ca^{2+} + 2CO_{2(g)}$	$\log\left(\frac{a_{Ca^{2+}}}{a_{Mg^{2+}}}\right) = -12.9 - 2 \cdot \log f_{CO_2}$
$2CaCO_{3(s)} + Mg^{2+} \rightleftharpoons CaMg(CO_3)_{2(s)} + Ca^{2+}$	$\log\left(\frac{a_{Ca^{2+}}}{a_{Mg^{2+}}}\right) = \log K = -0.3605$
$CaMg(CO_3)_{2(s)} + Mg^{2+} \rightleftharpoons 2MgCO_{3(s)} + Ca^{2+}$	$\log\left(\frac{a_{Ca^{2+}}}{a_{Mg^{2+}}}\right) = \log K = -0.5293$
$2CaMg(CO_3)_{2(s)} + Mg^{2+} \rightleftharpoons CaMg_3(CO_3)_{4(s)} + Ca^{2+}$	$\log\left(\frac{a_{Ca^{2+}}}{a_{Mg^{2+}}}\right) = \log K = -2.1852$

The stability of each carbonates at constant temperature and pressure can be displayed by a plot of the molality ratio of calcium and magnesium which is given in table 6 with respect to fugacity of carbon dioxide [91]. Thermodynamic equilibrium constants, at 25°C of the chemical reactions used to construct the log-log diagram of Ca/Mg activity ratio vs. CO_2 fugacity are given in Table 8.

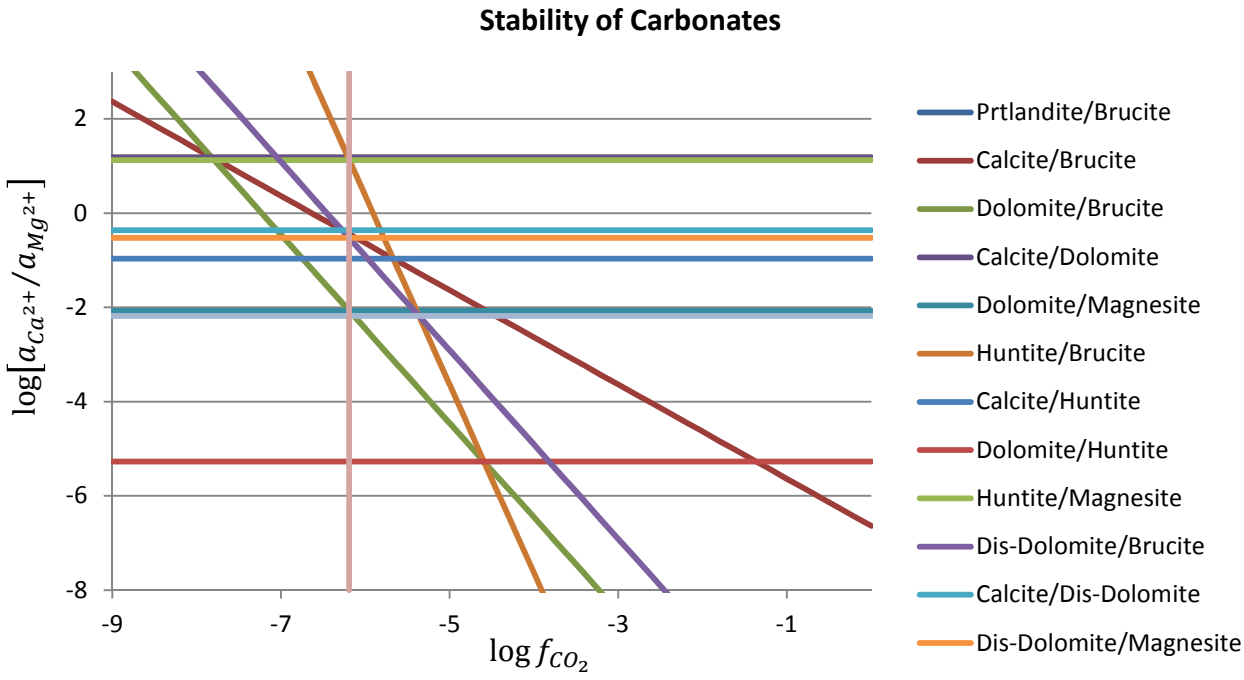

Figure 20 Log-log plots of the Ca^{2+}/Mg^{2+} activity ratio vs. CO_2 fugacity, showing the stability relations in the CaO-MgO-CO_2-H_2O system at 25°C. This figure also reflects the effect of pH on the activity ratio because fugacity and pH are directly related through equations (3-59) and (3-60).

According to the Schreinemakers' rule "Phase boundaries, when produced, must extend into fields with a higher number of phases or in other terms, no divariant assemblage can be stable within a sector that makes an angle of more than 180° measured between any two univariant lines in the same bundle [92, 93].

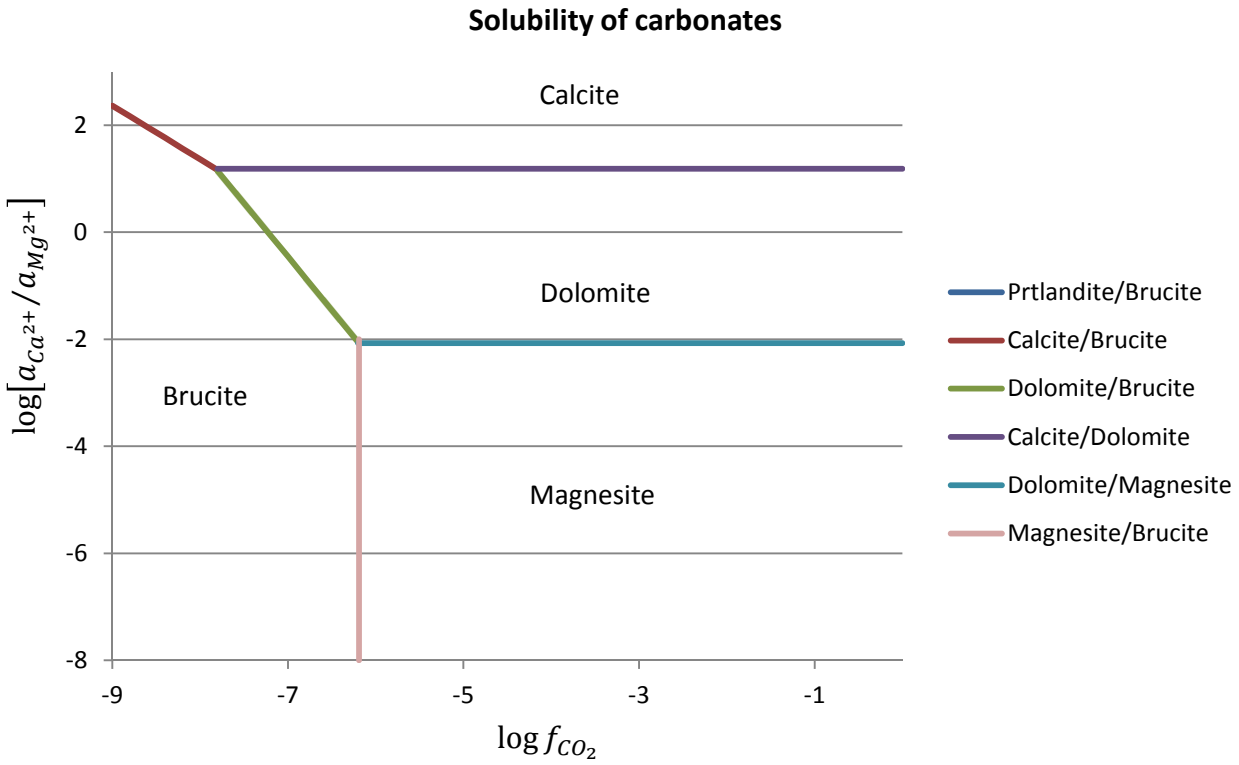

Figure 21. Log-log plots of the Ca^{2+}/Mg^{2+} activity ratio vs. CO_2 fugacity, showing the stability relations in the CaO-MgO-CO_2-H_2O system at 25°C.

As could be seen in Figure 21 the main carbonate minerals are Ca-, Mg- and Ca-Mg-carbonates. Calcite and dolomite are the two most stable carbonate minerals under reservoirs conditions. In deep reservoirs conditions, the conditions of temperature and pressure typical of saline aquifers, i.e. 50 to 100˚C and 1-500 bar, respectively. Fugacity values of CO_2 are high, so calcite and dolomite are two wide spread minerals [1].

4.2. The product solid phase

Formal description of calcite and dolomite structure (Reeder, 1990) is given in Table 9.

Table 9. Cell parameters and positional parameters of dolomite refer to the Lake Arthur specimen of composition $[Ca_{1.00}][Mg_{0.99}\,Ca_{0.01}](CO_3)_2$ [89].

	Calcite	Dolomite
Class symmetry	Trigonal scalenohedral	Trigonal rhombohedral
Space group	$R\bar{3}c$ (No. 167)	$R\bar{3}$ (No. 148)
Unit cell	Hexagonal, rhombohedrally,centred	Hexagonal, rhombohedrally,centred
Cell contents	$6CaCO_3$	$3CaMg(CO_3)_2$
Cell parameters	a=b=4.9896 Å c=17.0610 Å	a=b=4.8069 Å c=16.0034 Å
Atom positions	Ca in 6 (b): 0, 0, 0 C in 6 (a):0, 0, 1/4 O in 18 (e): x, 0, ¼ X=0.2568	Ca in 3 (a): 0, 0, 0 Mg in 3 (b): 0, 0, ½ C in 6 (c): 0, 0, z_c O in 18 (f): x_O, y_O, z_O $z_C = 0.24282(4)$ $x_O = 0.24776(7)$ $y_O = -0.03525(7)$ $z_O = 0.24404(2)$

For any mineral, the volume of the unit cell, v_0 is given by (Pauling, 1970):

$$v_0 = abc(1 + 2\cos\alpha\cos\beta\cos\gamma - cos^2\alpha - cos^2\beta - cos^2\gamma)^{1/2} \quad 3\text{- }1$$

For the hexagonal crystal system: $\alpha = \beta = 90^\circ$ and $\gamma = 120^\circ$. Hence:

$$v_0 = abc(1 - cos^2 120)^{1/2} = 367.85\ Å^3 \quad 3\text{-}2$$

The molar volume v ($cm^3\ mol^{-1}$) can be computed by knowing the unit cell volume:

$$v = \frac{v_0 \times N_A \times 10^{-24}}{Z} = 36.92\ cm^3\ mol^{-1} \quad 3\text{-}3$$

here Z is the number of molecules in the unit cell which is 6 for calcite, N_A the Avogadro's number and 10^{-24} the transformation factor from $Å^3$ to cm^3. Then the density ρ can be determined:

$$\rho = \frac{MW}{v} = \frac{100.091}{36.92} = 2.71\ g\ cm^{-3} \quad 3\text{-}4$$

Parameters of calcite are related to its density. Since density of calcite is greater than density of brine; after the reaction between calcium ion and carbonate, it precipitates toward the bottom of the aquifers.

4.3. Conclusion

All the outcomes of the previous discussion are based on purely thermodynamic considerations. As long as the equilibrium reactions between each secondary species and the basis have been considered, any reaction written among the secondary species is redundant in order to find the consumption rate of CO_2 [13, 34]. Things might be different if the system does not attain stable chemical equilibrium, as assumed above. In this case, it is reasonable to assume that either huntite or calcite will form, depending on the Ca^{2+}/Mg^{2+} activity ratio. This possibility is shown in the log-log plots of Ca^{2+}/Mg^{2+} activity ratio with respect to the change in CO_2 fugacity of figure 21. Furthermore, geochemical reaction path modeling, tracing the change of aqueous solution compositions and speciation and minerals through time or reaction progress, is used in chapter 4 to assess the extent of water-aqueous-gas interactions under reservoirs conditions with appropriate ranges of temperature and pressure. According to the United States Geological Surveys (USGS) [46] respective parameters conforming to a general Arrhenius-type rate equation is applied to find the dissolution and precipitation rates.

Chapter 5: The kinetics of the mineral carbonation

5.1. Precipitation and Dissolution rate

Chemical equilibrium models can be used to describe properly reversible and fast reactions only. In contrast, a kinetic approach becomes necessary when dealing with irreversible reactions like precipitation of calcite involving dissolved CO_2 and carbonate. Precipitation rate constant can be calculated from the equilibrium constant and the dissolution rate constant:

$$K_{equilibrium} = \frac{k^{+}_{dissolution}}{k^{-}_{precipitation}} \qquad 4\text{- }1$$

5.2. Dissolution rate constant

Geochemical reaction path modeling, tracing the change of aqueous solution compositions and speciation and minerals through time or reaction progress, has been used to assess the extent of water-aqueous-gas interactions under reservoirs conditions with appropriate ranges of temperature and pressure. According to the United States Geological Surveys (USGS) [46] respective parameters conforming to a general Arrhenius-type rate equation is applied to find the dissolution and precipitation rates. According to Arrhenius equation for natural media:

$$k^{+}_{dissolution} = A\, exp\left(-\frac{E_a}{RT}\right) \quad \rightarrow \quad \log k^{+} = \log A - \frac{E}{2.3025\, RT} \qquad 4\text{- }2$$

Dissolution rate of minerals can also be affected by the pressure of the system. From what has been observed in figure 17 the greater the pressure above the brine the more acidic is the brine. Due to the production of carbonic acid, pH of the system decreases after dissolution of CO_2. The effect of pressure can be taken into account implicitly by extending the standard Arrhenius eq. with a pH based term, as posed by USGS:

$$\log k^{+} = \log A - \frac{E}{2.3025\, RT} - n \times pH \qquad 4\text{- }3$$

5.3. Precipitation rate of minerals

According to the table 10, dissolution rates of minerals can be calculated with respect to the pH of the system. On the other hand regarding to the Arrhenius equation dissolution rate can be expressed at different temperatures. By applying $\text{equation}\,(4-1)$ with respect to the equilibrium constant of each reaction, precipitation rate of minerals can be determined.

Table 10. USGS data for the kinetics of the minerals. [81]

	Acid Mechanism			**Neutral Mechanism**			**Base Mechanism**		
	[a]log k	**E**	**n**	**log k**	**E**		**log k**	**E**	**n**
Anorthite	-3.50	16.6	1.411	-9.12	17.8				
Calcite	-0.3	14.4	1.000	-5.81	23.5		-3.48	35.4	1.000

here, a. log rate constant k at 25°C and pH = 0, log mole m^{-2} s^{-1}, b. Arrhenius activation energy E, kJ $mole^{-1}$, c. Reaction order n with respect to H^+, d. Reported values for k and E from Incenhower and Dove (2000). The acidic, neutral, and basic regions were selected by Hellman (1994a) to be the ranges of pH 1.3 to 4.0, 5.6 to 8.2, and 8.6 to 10.3 respectively.

First let us find the pre-exponential factor for dissolution of calcite (According to the table 9 rate constant k at 25°C and pH = 0) by applying equation (4-3). The equilibrium constant of calcite is $10^{-8.3}$ at 25°C.

$$A = 167.6$$

Dissolution rate of calcite can also be affected by pH of the system. Whereas the effect of pressure is taken into account in Arrhenius equation:

$$\log k^{+}{}_{Calcite} = \log A - \frac{E}{2.3025\,RT} - n \times pH \qquad 4\text{-}4$$

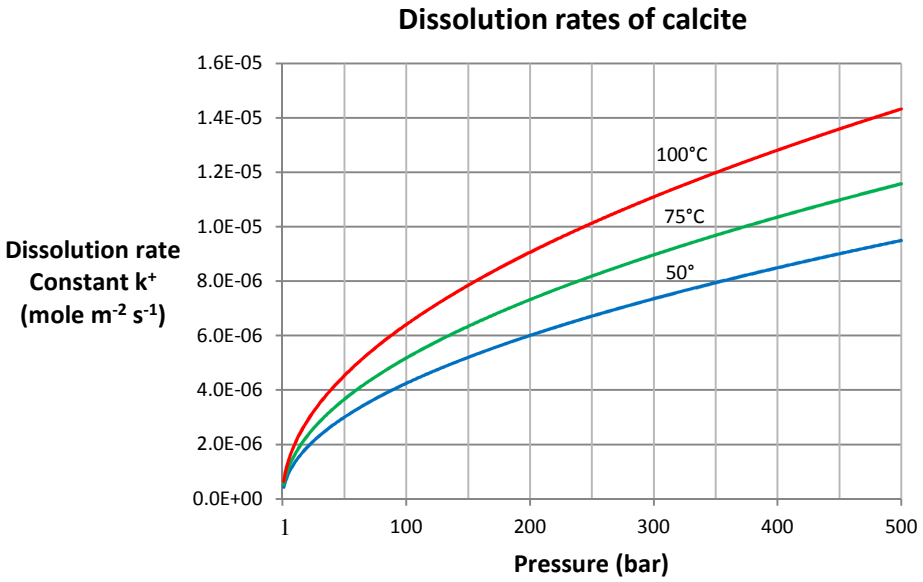

Figure 22. Dissolution rate of calcite in aqueous phase computed at 50, 75 and 100°C and variable pressures.

Figure 22, depicts the variation of dissolution rate of calcite with respect to the change in pressure. The dissolution rate of calcite has been found to increase with increase in pressure and temperature.

5.4. Precipitation rate of Calcite

Precipitation rate of calcite can be calculated from the equilibrium constant and the dissolution rate constant (equation 4-1):

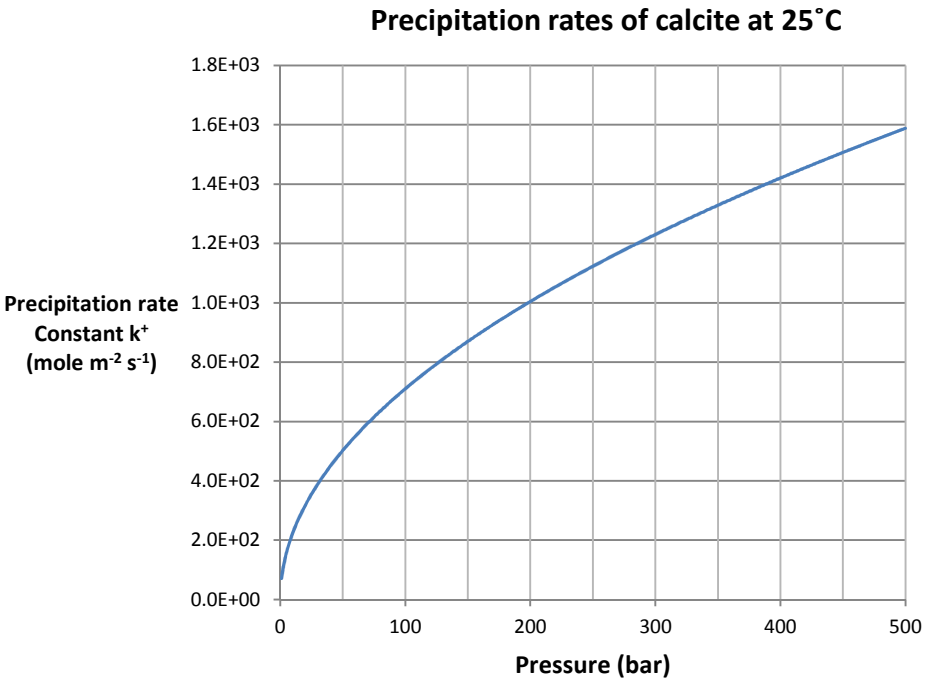

Figure 23. Precipitation rate of calcite in aqueous phase computed at 25°C and variable pressures.

Figure 23 depicts the variation of the precipitation rates of calcite at 25°C with viable pressue. The precipitation rate of calcite has been found to increase with increase in pressure and temperature. In order to store CO_2 in solid phase as $CaCO_3$, free calcium Ca^{2+} which provided by anorthite is also necessary. After finding the dissolution rate of anorthite, the rate-limiting in this process can be determined.

Pre-exponential factor for dissolution of anorthite can also be calculated by using equation (4-3):

$$A = 0.257$$

According to the Arrhenius equation, by considering effect of temperature, pressure and pH, dissolution rate of anorthite can be expressed by the equation (4-3):

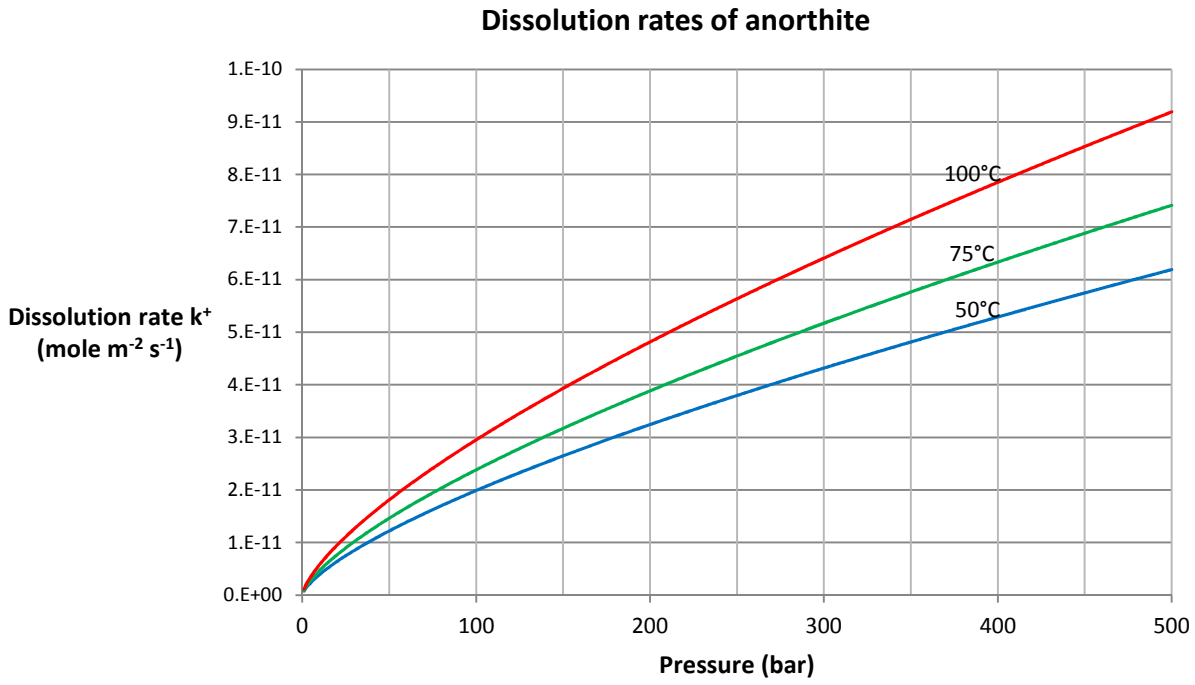

Figure 24. Dissolution rate of anorthite in aqueous phase computed at 50, 75 and 100°C and variable pressures.

Figure 24 depicts the variation of dissolution rate of anorthite with respect to the change in pressure. The dissolution rate of anorthite has been found to increase with increase in pressure and temperature.

5.5. Concluding remarks

Very few of these experiments have been investigated under CO_2 partial pressures of interest in geological CO_2 sequestration. Furthermore, most of the obtained laboratory rates are difficult to be compared with one another because of their dependence on either the adopted experimental conditions (i.e. pH and temperature ranges, composition and ionic strength of the solution, structural and compositional variability of the minerals, surface activation energy, etc.). The most available data on the kinetics of dissolution and precipitation from the USGS have been used to find the dissolution/precipitation of calcite and anorthite.

Chapter 6: Conclusion and Future work

The setup considered in this work consists of a two-phase region where CO_2-rich (supercritical) phase and H_2O-rich liquid brine phase coexist and are mutually soluble. In previous works, the researchers used experimental data to obtain the activity coefficients of CO_2 in saline aquifers. In this study, activity coefficients of CO_2 have been determined through the modified Redlich-Kwong equation. These values are calculated based on the fugacity of CO_2 calculated through the corresponding values of molar volume and thermodynamic equilibrium constants. The molar volumes recommended by NIST agree with the ones obtained in this research. It has been found that higher activity coefficients lead to decreasing mole fraction of CO_2 in aqueous phase.

From what have been observed in this study, it is found that the dissolution rate of anorthite is the rate-limiting process in sequestration of CO_2 under the conditions of temperature and pressure typical of saline aquifers, i.e. 50 to 100˚C and 1-500 bar, respectively. As long as, Ca^{2+} is available in brine, the reaction proceeds based on the precipitation rate of calcite. After all the dissolved Ca^{2+} has been consumed by the reaction with CO_3^{2-}, in order to store CO_2 as calcite, Ca^{2+} needs to dissolve out of the mineral surface for further reaction to take place. In this case, dissolution rate of anorthite dominates the net rate process. In order to store CO_2 via mineral trapping, both time and contact surface area play important roles. The consumption rate of CO_2, which has been expressed in terms of contact surface area, may prove to be vital for future work. Since, the dissolution rate of anorthite increases with the increase in pressure and temperature (figure 24), both pressure and temperature accelerate the consumption rate of CO_2. In other words, for a specific period of time, larger amount of CO_2 is trapped as solid phase at higher temperature and pressure. At higher pressures, the molar volume of CO_2 also decreases and leads to a greater density of CO_2. The solubility of CO_2 in liquid phase increases as pressure increases. However, temperature and salinity have inverse effects on the solubility of CO_2 in aqueous phase. Therefore, higher temperatures and salinities lead to decreasing solubility of CO_2. The consumption rate of CO_2 in aqueous phase increases with an increase in both the aquifer pressure and temperature, which is favorable for the mineral trapping of CO_2. However, with respect to solubility trapping of CO_2, in contrast to the beneficial effect of higher values of pressure, higher values of temperature show a detrimental effect.

The results related to the solubility of CO_2 are compared with experiments in figures 4, 11, 12 and 13. Differences between experimental and calculated results may arise due to factors not accounted for in the theoretical model including, i.e. variations in grain size, aquifer heterogeneity, diffusion, convection, primary and secondary mineral coatings, and secondary minerals that may lead to decreased porosity and permeability.Under these restrictions, mutual solubilities and the consumption rate of CO_2 in liquid phase reported by various sources are in good agreement with the results in this method.

Future work

In this study, the dynamics of moving fluid has not been considered. However, this study has provided data that would go hand in hand in providing both the right boundary conditions and for determining the appropriate reaction rates for the chemical reaction equations that go along with governing equations for the fluid dynamics. Thus the simulation of fluid flow and mineral reactions in a fracture within porous media can be achieved. The effects of convection, diffusion, and precipitation and dissolution reactions on the CO_2 sequestration when taken into account together may result in diverse flow features that need to be explored.

Nomenclature

Mg……..Magnesium

S …….. Entropy

V ……. Volume

$\mu_{i,\alpha}$ ……..… Chemical potentials of the *i*th chemical component in the phase α

$\varphi_{i,g}$ ……..…… Fugacity coefficient

P ……...……... Total gas pressure

$y_{i,g}$ ……..…... Molar fraction of the *i*th component in the gas phase g

$\gamma_{i,L}$ …… Activity coefficient

$x_{i,L}$ ……..... Molar fraction of the *i*th component in the liquid phase L

f_i^o ……..…. Fugacity of component *i* in a condition of reference which is called standard state

s_k ……..……Molar entropy of substance *k*

v_k ……..…….. Molar volume of substance *k*

T ……..…….. Temperature

P ……..…….. Pressure of interest

Tr ……..… Temperature of a given arbitrarily but suitably chosen reference state

Pr ……..…… Pressure of a given arbitrarily but suitably chosen reference state

ΔG ……..…….. Gibbs free energy

ΔG^o ……..……Standard state Gibbs free energy of the reaction

v_i ……..……. Stoichiometric coefficient

N_A …… The Avogadro's number

k_B ……..…..…….. Boltzmann's constant, $1.38066 \times 10^{-23}\ J\ K^{-1}$

ρ ……..…… Density of CO_2

MW …….. Molecular weight

Z ……..…..…… Compressibility factor

$\emptyset$ ……..……. Fugacity coefficient of CO_2

$K_{T,P}$ ……...…… Equilibrium constants

$\bar{V}_i$ ……..…… Average molar volume

$\gamma_{\pm}$ …..…. Mean stoichiometric activity coefficient of a completely dissociated binary electrolyte

$\bar{I}$ ……..…… True ionic strength

e ……..…… Absolute electronic charge

ε_0 ……..…… Permittivity of free space

ε …… Relative permittivity of water

k …… Salting-out coefficient

m ……...…… Molality of NaCl

K_H° ……..……..……...Henry's law coefficients for pure water as solvent

K_H …….. Henry's law coefficients for the saline solution

n^* ……. the sum of the molalities of the solute species

$K_{H,CO_2,sol}$ ……..….... Henry's Law coefficients for the saline solution

$K_{H,CO_2,water}$ ……..Henry's Law coefficients for pure water as solvent

y_i …..…….…….…….. Mole fraction of the *i*th component in the gas mixture

Z ……...……. is the number of molecules in the unit cell

N_A ……..…… The Avogadro's number

K_{sp} ……. Thermodynamic solubility product of calcite

A_a …….…… Pre-exponential factor in Arrhenius equation

E_a ……...……. Activation energy term

R ……...…… Universal gas constant

$r_{c,t=0}$ …….. Average radius of the crystals at time "zero"

C_B ……..…….. Concentration of the solute in the aqueous solution

C_s ……...……. Concentration close to the crystal surface

χ_i …….…… Electronegativity of the *i*th element

x_{CO_2} …….……. Mole fraction of CO_2 in solution

a ……..…… log rate constant k at 25°C and pH = 0, log mole m^{-2} s^{-1} for use with (eqn 135)

b. …….……. Arrhenius activation energy E, kJ $mole^{-1}$

c. ……..…… Reaction order n with respect to H^+

d. ……...…….. Reported values for k and E from Incenhower and Dove (2000)

$CaAl_2Si_2O_8$. ……..……Anorthite

H_2CO_3. ……...…….Carbonic acid

HCO_3^-. ……..…….Bycarbonate

CO_3^{2-}. ……....Carbonate

C_T. ……Total Concentration

Da. ……Damkohler number

Appendix 1

The chemical potential

For each chemical component *i*, the chemical potential μ_i, in a homogeneous single phase of different chemical components, is equal to the partial derivative of the Gibbs free energy of the system, G, with respect to the moles n_i of *i*th component, at constant pressure *P*, temperature *T*, and composition of all constituents except *i*:

$$\mu_i = \left(\frac{\partial G}{\partial n_i}\right)_{P,T,n_j}$$

The fundamental independent variables for G, as indicated by the relation:

$$dG = -SdT + VdP$$

where, *S* is the entropy and *V* the volume.

Certain thermodynamic requirements exist for establishment of equilibrium conditions between components in different phase of heterogeneous systems. The first important requirement is that these phases must be equal in temperature for thermal equilibrium to exist. In other words, there is no net interphase heat flow at equilibrium. Second and more important condition of phase equilibria is that the chemical potential of each component must be the same in each phase. There are two ideal solution laws that govern the equilibrium between gas and liquid phases. The first of these, Raoult's law, governs the behavior of solid or liquid substances with respect to vapor phase. The second, Henry's law, governs the behavior of extremely dilute aqueous solution of dissolved solutes with respect to air (Luigi Marini, 2007). For a heterogeneous system, i.e. consisting of two or more phases, the equilibrium distribution of a given chemical component *i* between two phases α and β is described by:

$$\mu_{i,\alpha} = \mu_{i,\beta}$$

where $\mu_{i,\alpha}$ and $\mu_{i,\beta}$ are the chemical potentials of the *i*th chemical component in the two phases α and β, respectively [4].

Fugacity and activity coefficients

For applying this equation it is convenient to introduce two additional functions: the activity and the fugacity. Fugacity and activity coefficients both describe how real mixtures deviate from ideal mixtures. Both fugacity coefficient $\varphi_{i,g}$ and activity coefficient $\gamma_{i,L}$ approach 1 when real mixtures approach the ideal behavior. What exactly is an ideal gas? An ideal gas is one that exactly conforms to the kinetic theory. The kinetic theory, as stated by Rudolf Clausius in 1857, has five key points:

Gases are made of molecules in constant, random movement. Gases like Argon have 1-atom molecules.

The large portion of the volume of a gas is empty space. The volume of all gas molecules, in comparison, is negligible.

The molecules show no forces of attraction or repulsion.

No energy is lost in collision of molecules; the impacts are completely elastic.

The temperature of a gas is the average kinetic energy of all of the molecules.

$$\frac{\varphi_{i,g} y_{i,g} P}{f_i^o} = \gamma_{i,L} x_{i,L}$$

where, P is total gas pressure; $\varphi_{i,g}$ is the fugacity coefficient and $y_{i,g}$ is the molar fraction of the ith component in the gas phase g. $\gamma_{i,L}$ is the activity coefficient and $x_{i,L}$ is the molar fraction of the ith component in the liquid phase L. f_i^o is the fugacity of component i in a condition of reference which is called standard state. In general, however, we have to know the relations describing how $\varphi_{i,g}$ and $\gamma_{i,L}$ depend on temperature, pressure and composition:

$$\varphi_{i,g} = f(T, P, y_1, y_2, y_3, \dots) \quad \text{and} \quad \gamma_{i,g} = f(T, P, x_1, x_2, x_3, \dots)$$

The chemical potential should be found by measurable variables, temperature, pressure and composition. But finding absolute values of the chemical potential is difficult to be measured. To

overcome this difficulty, variations in the chemical potential need to be calculated. This is the equation that links the chemical potential of given substance *k* to temperature and pressure.

$$d\mu_k = -s_k dT + v_k dP$$

here, s_k and v_k are the molar entropy and the molar volume of substance *k*, respectively. By integrating of the equation:

$$\mu_{k,T,P} = \mu_{k,Tr,Pr} - \int_{Tr}^{T} s_k dT + \int_{Pr}^{P} v_k dP$$

where, *T* and *P* are the temperature and pressure of interest, *Tr* and *Pr* are the temperature and pressure of a given arbitrarily but suitably chosen reference state, respectively.

If the thermal and volumetric properties of substance *k* are known over the temperature interval *Tr* to *T* and the pressure interval *Pr* to *P*, respectively, then it is possible to compute the two integrals $\int_{Tr}^{T} s_k dT$ and $\int_{Pr}^{P} v_k dP$, but the term $\mu_{k,Tr,Pr}$ the chemical potential at the reference state is still unknown. This requires measuring the molar volumes down to sufficiently low pressure. However, under these conditions the molar volume becomes very large and difficult to be measured. In addition, from the point of view of calculus, the integral $\int \vartheta dP$ is difficult to evaluate for $\vartheta \to \infty$. To overcome these difficulties, it is convenient to define the function:

$$\vartheta_{ideal} - \vartheta_{real} = \frac{RT}{P} - \vartheta$$

The chemical potential at standard state is usually indicated by the superscript ^{o} and it is related to the activity, a_k, by the following equation:

$$\mu_k = \mu_k^o + RT \ln a_k$$

For gases, the standard state convention is the perfect gas at 1 bar and for aqueous species; the standard state convention is one molal solution with infinite dilution at any pressure and temperature. In other words, adopted standard-state convention has nothing to do with real one molal solution (Luigi Marini, 2007).

Conventions

1) Pure solids and liquids have unit activity at all pressures and temperatures. Pure gases have unit activity at 1 bar and any temperature. Aqueous solutes have unit activity in one molal solution at any pressure and temperature.

2) Under standard state conditions the chemical potential of any element in its most stable phase is equal to zero, for example, the proton and electron in aqueous solution have the chemical potential of zero [5].

For a pure, ideal gas k:

$$\left[\frac{\partial \mu_k}{\partial P}\right]_T = \vartheta_k$$

From the ideal gas law:

$$\vartheta_k = \frac{RT}{P} \quad \rightarrow \quad \frac{\partial \mu_k}{\partial P} = \frac{RT}{P} \quad \rightarrow \quad \int \partial \mu_k = \int RT \frac{\partial P}{P} \quad \rightarrow \quad \mu_k - \mu_k^o = RT[\ln P - \ln P^o]$$

$$\mu_k = \mu_k^o + RT \ln \frac{P}{P^0}$$

In other words, the change in the abstract chemical potential is related to the change in a physically measurable variable, the pressure. Since this equation is true only for a pure, ideal gas, Lewis defined a function, called fugacity. He stated that for any chemical component *i* in any phase, either a gas, a liquid or a solid, pure or mixed, ideal or not ideal, the change in chemical potential during an isothermal transition from fugacity f_i^o to fugacity f_i is:

$$\mu_i - \mu_i^o = RT \ln \frac{f_i}{f_i^o}$$

The ratio $\frac{f_i}{f_i^o}$ was termed activity by Lewis.

The fugacity is equal to the pressure for a pure, ideal gas and it is equal to the partial pressure $P \times y_i$ for the *i*th component of a mixture of ideal gases. Since both pure gases and gas mixtures approach the behavior of ideal gases of very low pressure.

For pure gases:

$$\lim_{p\to 0}\frac{f}{p}=1 \quad \text{and for gas mixture:} \qquad \lim_{p\to 0}\frac{f_i}{P\times y_i}=1$$

From what has been discussed above at constant temperature, the chemical potential can be expressed by following equation:

$$\mu_i-\mu_i^o=RT\ln\frac{f_i}{f_i^o}=-\int_{Tr}^{T}s_k dT+\int_{Pr}^{P}v_k dP$$

$$\vartheta_{ideal}-\vartheta_{real}=\frac{RT}{P}-\vartheta$$

$$-\int_{Tr}^{T}s_k dT=0 \quad \rightarrow \quad \ln\frac{f_i}{f_i^o}=\frac{1}{RT}\int_{Pr}^{P}v_k dP=\frac{1}{RT}\int_{p\to 0}^{P}\left(\frac{RT}{P}-\vartheta\right)dP$$

The fugacity of a pure gas is related to pressure through the following equation:

$$f=\varphi.P$$

where, φ is the fugacity coefficient of the gas. For a gas mixture, the fugacity of the *i*th gaseous component is related to its partial pressure by:

$$f_i=\varphi_i.P.y_i$$

Chemical equilibrium

Thermodynamics is applied at chemical equilibrium [7]. However many natural systems are far from chemical equilibrium, either initially or during their evolution. Chemical equilibrium for a given reaction is expressed by following equation:

$$\Delta G = \Delta G^o + RT \ln \prod_i a_i^{v_i}$$

where, ΔG is Gibbs free energy and ΔG^o is the standard state Gibbs free energy of the reaction, the $RT \ln \prod_i a_i^{v_i}$ term involves the activities of reactants and products of the reaction, each elevated to the corresponding stoichiometric coefficient, v_i. This is a negative number for reactants and positive number for products.

At equilibrium:

$$\Delta G = 0 \quad \rightarrow \quad \Delta G^o = -RT \ln K$$

According to Nordstorm and Munoz 1985 [6], Anderson and Crerar 1993 [7].

$$K = \prod_i a_i^{v_i}$$

References

1. Marini, L. (2006). *Geological sequestration of carbon dioxide.* Elsevier.
2. Ed's J. T. Houghton, Y. Ding, D. J. Griggs et al., The Carbon Cycle and Atmospheric Carbon Dioxide, I.C. Prentice, Tim Lenton , et al. In Climate Change 2001: The Scientific Basis, CUP, Cambridge, pp 188-237.
3. Lasaga, A. (1998). Kinetics theory. *Earth science*.
4. http://www.thewe.cc/weplanet/news/air/co2_record_high_levels_in_the_atmosphere.htm
5. http://www.co2crc.com.au/
6. Michael, BC; Donazzi, A; Schmidt, LD (2005). Effects of H_2O and CO_2 addition in catalytic partial oxidation of methane on Rh. *Journal of catalysis*, Volume: 265, Issue: 1, Pages: 117-129
7. Watson, T. L., & Bachu, S. (2009). Evaluation of the Potential for Gas and CO_2 Leakage Along Wellbores. *SPE Drilling & Completion, 24*(1), 115-126.
8. Bachu, S., & Adams, J. (2003). Sequestration of CO_2 in geological media in response to climate change: capacity of deep saline aquifers to sequester CO_2 in solution. *Energy Conversion and Management, 44*(20), 3151-3175.
9. Socolofsky, S. A., & Adams, E. (2002). Multi-phase plumes in uniform and stratified crossflow. *Hydraulic research, 40*(6), 661-672.
10. Yunzhen, L., & Tao, H. (2010). The Study on Supercritical Multi-Phase Fluid in Carbon Dioxide Sequestration. *Bioinformatics and Biomedical Engineering (iCBBE), 2010 4th International Conference on*, (pp. 1 - 4). Chengdu.
11. Kerrick, D., & Jacobs, G. (1981). A modified Redlich-Kwong equation for H_2O, CO_2, and H_2O- CO_2 mixtures at elevated pressures and temperatures. *American Journal of Science, 281*, 735-767.
12. P. Debye and E. Hückel (1923). "The theory of electrolytes. I. Lowering of freezing point and related phenomena". Physikalische Zeitschrift 24: 185–206

13. Spycher, N., & Pruess, K. (2005). CO_2-H_2O mixtures in the geological sequestration of CO_2. II. Partitioning in chloride brines at 12–100°C and up to 600 bar. *Geochimica et Cosmochimica Acta, 69*(13), 3309-3320.
14. MacMinn, C., Szulczewski, M., & Juanes, R. (2010). CO_2 migration in saline aquifers. Part 1. Capillary trapping under slope and groundwater flow. *Journal of fluid mechanics, 662*, 329-351.
15. Noh, M. H. (2003). *Reactive Transport Modeling in Fractures and Two-phase Flow.*
16. http://www.natureef.com/calcium1.htm
17. (2010). *Encyclopædia Britannica.* Chicago.
18. Sabine, C. L., Feely, R. A., Gruber, N., Key, R. M., Lee, K., Bullister, J. L., et al. (2004). The Oceanic Sink for Anthropogenic CO_2. *Science, 305* (5682), 367-371.
19. http://www.sciencemag.org/cgi/content/short/305/5682/367".
20. "Ocean Acidification Network". http://ioc3.unesco.org/oanet/FAQacidity.html.
21. Garcia, J. E. (2001). *Density of aqueous solutions of CO_2.* Ernest Orlando Lawrence Berkeley National Laboratory, Berkeley, CA (US).
22. O'Leary, M. H. (1984). Measurement of the isotope fractionation associated with diffusion of carbon dioxide in aqueous solution. *J. Phys. Chem, 88*(4), 823-825.
23. R. A. Berner (1978)**.** Rate control of mineral dissolution under Earth surface conditions. American Journal of Science, Vol. 278, November 1978, P.1235-1252; doi:10.2475/ajs.278.9.1235.
24. Chou, L., Garrels, R. M., & Wollast, R. (1989). Comparative study of the kinetics and mechanisms of dissolution of carbonate minerals. *Chemical Geology, 78*(3-4), 269-282.
25. Aagaard, P., & Helgeson, H. C. (1982). Thermodynamic and kinetic constraints on reaction rates among minerals and aqueous solutions; I, Theoretical considerations. *American Journal of Science, 282*, 237-285.
26. Herbert S. Harned, Raymond Davis Jr (1943). The Ionization Constant of Carbonic Acid in Water and the Solubility of Carbon Dioxide in Water and Aqueous Salt Solutions from 0 to 50°C. *J. Am. Chem. Soc.*, 1943, 65 (10), pp 2030–2037, DOI**:** 10.1021/ja01250a059.
27. Kissinger, H. E. (1957). Reaction Kinetics in Differential Thermal Analysis. *Anal. Chem, 29*(11), 1702–1706.

28. Andrew McLeish (2001), Geological science. ISBN: 0-17-448221-3.Impact of Capillary Pressure, Salinity and In situ Conditions on CO_2 Injection into Saline Aquifers, H. Alkan, Y. Cinar and E. B. Ülker, Transport in Porous Media Volume 84, Number 3, 799-819
29. Tianfu Xu, John A. Apps, and Karsten Pruess(2002), Reactive Geochemical Transport Simulation to Study Mineral Trapping for CO_2 Disposal in Deep Saline Arenaceous Aquifers.
30. Yang, D., Tontiwachwuthikul, P., & Gu, a. Y. (2005). Interfacial Interactions between Reservoir Brine and CO_2 at High Pressures and Elevated Temperatures. *Energy Fuels, 19*(1), 216–223.
31. Stefan Bachu, D. B. (2009). Interfacial Tension between CO_2, Freshwater, and Brine in the Range of Pressure from (2 to 27) MPa, Temperature from (20 to 125) °C, and Water Salinity from (0 to 334000) mg·L−1. *J. Chem. Eng. Data, 54*(3), 765–775.
32. Kwak, T., & Mansoori, G. (1986). Van der waals mixing rules for cubic equations of state. Applications for supercritical fluid extraction modelling. *Chemical Engineering Science, 41*(5), 1303-1309.
    A. Kumar, M. N. (2005). Reservoir Simulation of CO_2 Storage in Deep Saline Aquifers. *SPE Journal, 10*(3), 336-348.
33. Mucci, A. (1983). The solubility of calcite and aragonite in seawater at various salinities, temperatures, and one atmosphere total pressure. *American Journal of Science, 283*, 780-799.
34. Curtiss, C. F., & Bird, R. B. (1996). Multicomponent Diffusion in Polymeric Liquids. *Proc. Natl. Acad. Sci., 93*(15), 7440-7445,.
35. Kramers, L., & Hangx, S. (2006). *Solubility and dissolution rate of CO_2 in water.* HPT Laboratory, Department of Earth Sciences.
36. Gordon, L., & Jones, L. (1973). The effect of temperature on carbon dioxide partial pressures in seawater. *Marine Chemistry, 1*(4), 317-322.
37. S.J.T.Hangx(2005), Behavior of the CO_2-H_2O system and preliminary mineralization model and experiments, HPT Laboratory, Department of Earth Sciences Utrecht University.

38. H. Berg(1983),"Random Walks in Biology", Ch. 1, 2 (Princeton University Press, 1983) R. Feynman, "Lectures on Physics", Vol. 1, Ch.43
39. Frank, M.J.W. and Kuipers, J.A.M. and Swaaij van, W.P.M. (1996) Diffusion Coefficients and Viscosities of $CO_2 + H_2O$, $CO_2 + CH_3OH$, $NH_3 + H_2O$, and $NH_3 + CH_3OH$ Liquid Mixtures. Journal of Chemical & Engineering Data, 41 (2). pp. 297-302. ISSN 0021-9568
40. Xu, Tianfu;, Apps, John A.; Pruess, Karsten(2001), Analysis of mineral trapping for CO_2 disposal in deep aquifers, , 07-20-2001, Lawrence Berkeley National Laboratory
41. Herbert S. Harned, Raymond Davis Jr(1943). The Ionization Constant of Carbonic Acid in Water and the Solubility of Carbon Dioxide in Water and Aqueous Salt Solutions from 0 to 50°, *J. Am. Chem. Soc.,* 1943, 65 (10), pp 2030–2037
42. Lagneau, V., Pipart, A., & Catalette, H. (2005). Reactive Transportmodelling and Long Term Behaviour of CO_2 Sequestration in Saline Aquifers. *Oil & Gas Science and Technology - Rev. IFP, 60*(2), 231-247.
43. Hellevang, H. (2006). Interactions between CO_2, saline water and minerals during geological storage of CO_2. The University of Bergen.
44. , W.K. O'Connor, D.C. Dahlin, G.E. Rush, S.J. Gerdemann, L.R. Penner, and D.N. Nilsen, (2005). Aqueous mineral carbonation.
45. Bird, R. B., Lightfoot, E. N., & Stewart, W. E. (2006). *Transport Phenomena.* John Wiley & Sons Inc.
46. C, B., Michael, Donazzi, A., & Schmidt, L. D. (2009). Effects of H_2O and CO_2 addition in catalytic partial oxidation of methane on Rh. *Catalysis, 265*(1), 117-129.
47. Bachu, S., W.D. Gunter, and E.H. Perkins. (1994). Aquifer disposal of CO_2: Hydrodynamic and mineral trapping. Energy Conversion and Management 35(4):269–279.
48. Benson, S. and D. Thomas (eds.). (2005). Carbon Dioxide Capture and Storage in Deep Geologic Formations – Results from the CO_2 Capture Project. Volume 2. Elsevier, London.

49. Haszeldine, R.S. (2006). Deep geological CO_2 storage: Principles reviewed, and prospecting for bio-energy disposal sites. Mitigation and Adaptation Strategies for Global Change 11(2):377-401.
50. Johnson, J. W., Nitao, J. J., Steefel, C. I., & Knauss, K. G. (n.d.) (2004). Reactive transport modeling of geologic CO_2 sequestration in saline aquifers: the influence of intra-aquifer shales and the relative effectiveness of structural, solubility, and mineral trapping during prograde and retrograde sequestration. Livermore, CA: Lawrence Livermore National Laboratory Geosciences and Environmental Technologies Division.
51. Kolak, J.J. and R.C. Burruss. (2003). An organic geochemical assessment of CO_2-coal interactions during sequestration. In Second Annual Conference on Carbon Sequestration. Alexandria, VA. pp. 5-8. May.
52. NASCENT. (2005). Natural Analogues for the Storage of CO_2 in the Geological Environment. IEA Greenhouse Gas R&D Programme. Technical Report 2005/06. Available: http://www.ieagreen.org.uk/2005.html. Accessed 12/7/2007.
53. Van der Meer, L. (1995). The CO_2 storage efficiency of aquifers. *Energy Conversion and Management, 36*(6-9), 513–518.
54. Zhang, Y. M. (2006). *System-level modeling for geological storage of CO_2.* Lawrence Berkeley National Laboratory, Berkeley, CA.
55. Zhang, G., Spycher, N., Sonnenthal, E., Steefel, C. And Xu, T., (2008). Modeling reactive multiphase flow and transport of concentrated solutions, Journal of Nuclear Technology, 164(2), 180 – 195.
56. Sengor, S. S., Spycher, N., Ginn, T. R., Sani, R. K., & Peyton, B. (2007). Biogeochemical reactive-diffusive transport of heavy metals in Lake Coeur d'Alene sediments. *Applied Geochemistry, 22*(12), 2569-2594.
57. Xu, T., Sonnenthal E., Spycher N., and Pruess, K., (2006), TOUGHREACT - A simulation program for non-isothermal multiphase reactive geochemical transport in variably saturated geologic Media: applications for geothermal injectivity and CO_2 geologic sequestration. Computers and Geosciences, 32, 145-165.

58. Spycher N. and Pruess K., (2005). CO_2-H_2O Mixtures in the Geological Sequestration of CO_2. II. Partitioning in chloride brines at 12-100°C and up to 600 bar. Geochimica Cosmochim. Acta, 69, 3309-3320.
59. Spycher, N., Pruess, K., & Ennis-King, J. (2003). CO_2-H_2O mixtures in the geological sequestration of CO_2. I. Assessment and calculation of mutual solubilities from 12 to 100°C and up to 600 bar. *Geochimica et Cosmochimica Acta, 67*(16), 3015-3031.
60. McQuarrie, Donald A. and Simon, John D. (1999). *Molecular Thermodynamics*. University Science Books. ISBN 1-891389-05-X. page 55
61. Fournier, R. O. (1985). Carbonate transport and deposition in the epithermal environment. *Economic Geology, 2*, 63-72.
62. Gilbert Newton Lewis (1901), The Law of Physico-Chemical Change, , Vol. 37, No. 3.
63. Brown, Theodore L., H. Eugene LeMay, Jr. and Bruce E. Burston (1994), *Chemistry: The Central Science*, Englewood Cliffs, NJ: Prentice Hall, Inc.
64. Dorin, Henry, Peter E. Demmin, and Dorothy L. Gabel (1989). *Prentice Hall Chemistry: The Study of Matter*, Needham, Massachusetts and Englewood Cliffs, New Jersey: Prentice Hall, Inc.
65. J. Willard Gibbs (Oct 1993), The Scientific Papers of J. Willard Gibbs, Vol. 1: Thermodynamics.
66. Nordstorm, D. K., & Munoz, J. L. (1986). Geochemical thermodynamics. *Geol. Mag, 123*(4), 459-472.
67. Greg M. Anderson and David A. Crerar (Jun 17, 1993), Thermodynamics in Geochemistry: The Equilibrium Model.
68. R Span, W. W. (1996). A New Equation of State for Carbon Dioxide Covering the Fluid Region from the Triple-Point Temperature to 1100 K at Pressures up to 800 MPa. *Journal of Physical and Chemical Reference Data, 25*(6), 1509-1596.
69. Youngil, K. (2007). Equation of state for carbon dioxide. *Journal of mechanical science and technology, 21*(5), 799-803.
70. Helgeson, H. C., Kirkham, D. H. and Flowers, G. C., (1981). Theoretical prediction of the thermodynamic behavior of aqueous electrolytes at high pressures and temperatures. IV. Calculation of activity coefficients, osmotic coefficients, and apparent molal and

standard and relative partial molal properties to 600degrees C and 5 Kb. *Am. J. Sci*., 281, 1249-1516.

71. Effenberger, H., Mereiter, K., & Zemann, J. (1980). Crystal structure refinements of magnesite, calcite, rhodochrosite, siderite, smithonite, and dolomite, with discussion of some aspects of the stereochemistry of calcite type carbonates. *156*, 233-243.
72. Loerting, T., Tautermann, C., Kroemer, R., Kohl, I., Mayer, E., Hallbrucker, A., et al. (2001). On the Surprising Kinetic Stability of Carbonic Acid. *Angew. Chem. Int. Ed., 39*, 891-895.
73. Welch, M. J., Lipton, J. F., & Seck, J. A. (1969). Tracer studies with radioactive oxygen-15. Exchange between carbon dioxide and water. *J. Phys. Chem., 73*(335), 3351.
74. Jolly, W. L. (1991). *Modern Inorganic Chemistry* (2nd ed.). New York: McGraw-Hill.
75. Moore, M. H., & Khanna, R. (1991). Infrared and Mass Spectral Studies of Proton Irradiated H_2O+CO_2 Ice: Evidence for Carbonic Acid Ice: Evidence for Carbonic Acid. *Spectrochimica Acta*, 255-262.
76. W. Hage, K. R. Liedl; Mayer, E.; Hallbrucker, A; Mayer, E (1998). "Carbonic Acid in the Gas Phase and Its Astrophysical Relevance". Science 279 (5355): 1332–1335. doi:10.1126/science.279.5355.1332. PMID 9478889.
77. Hage, W.; Hallbrucker, A.; Mayer, E. (1993). "Carbonic Acid: Synthesis by Protonation of Bicarbonate and Ftir Spectroscopic Characterization Via a New Cryogenic Technique". J. Am. Chem. Soc. 115: 8427–8431. doi:10.1021/ja00071a061.
78. Hage, W.; Hallbrucker, A.; Mayer, E. (1995). "A Polymorph of Carbonic Acid and Its Possible Astrophysical Relevance". J. Chem. Soc. Farad. Trans. 91: 2823–2826. doi:10.1039/ft9959102823.
79. Enick, R. M., & Klara, S. M. (1990). CO_2 solubility in water and brine under reservoir conditions. *Chemical Engineering Communications, 90*(1), 23-33.
80. Hellevang, H., Aagaard, P., Oelkers, E.H., and Kvamme, B., (2005). Can dawsonite permanently trap CO_2? *Environmental Science and Technology*, 39, 8281-8287.
81. James L. Palandri and Yousif K. Kharaka (2004), a compilation of rate parameters of water-mineral interaction kinetics for application to geochemical modeling. U.S. Geological Survey, open file report 2004-1068.

82. Redfield, A.C., Ketchum, B.H. and Richards, F.A. (1963) The influence of organisms on the composition of sea-water. In: Hill, M.N. (ed),*The Sea.* New York: Wiley, pp. 26-77.
83. Angus, S., Armstrong, B. and de Reuck, K.M. (1976) *International Thermodynamic Tables of the Fluid State-3 Carbon Dioxide.* New York: Pergamon.
84. Span, P. and Wagner, W. (1996) A new equation of state for carbon dioxide covering the fluid region from the trople point temperature to 1100K at pressures up to 800mpa. *J. Phys. Chem. Ref.* Data, 25-6, 1509-1596.
85. Spycher, N. and Pruess, K. and Ennis-King, J. (2003) CO_2-H_2O mixtures in the geological sequestration of CO_2. I. Assessment and calculation of mutual solubilities from 12 to 100°C and up to 600 bar. *Geochim, Cosmochin. Acta,* 67, 3015-3031.
86. Ellis, A. J. and Golding, R.M. (1963) The solubility of carbon dioxide above 100°C in water and in sodium chloride solutions. *Am. J. Sci.* 261, 47-60.
87. Helgeson , H.C., Kirkham, D.H. and flowers, G.C. (1981). Calculation of activity coefficients, osmotic coefficients and relative partial molar properties to 600°C and 5kb. *Am. J. Sci.,* 281, 1249-1516.
88. Prausnitz, J.M., Lichtenthaler, R.N. and Gomes de Azevedo, E. (1999) *Molecular Thermodynamics of fluid phase Equilibria,* 3rd ed. Upper Saddle River, NJ: Prentice-Hall, 860pp.
89. Reeder, R.J. (1990) Crystal chemistry of the rhombohedral carbonates. In: Reeder, R.J. (ed.), *Carbonates: Mineralogy and Chemistry, Reviews in Mineralogy,* Mineralogical Society of America, 2nd printing, 11, 1-47.
90. Wenk, H.-R., Barber, D.J. and Reeder, R.J. (1990) Microstructures in carbonates. IN: Reeder, R.J. (ed.), *Carbonates: Mineralogy and Chemistry, Reviews in Mineralogy,* Mineralogical Society of America, 2nd printing, 11, 301-367.
91. Langmuir, D. (1984) Physical and chemical characteristics of carbonate water. In.: Lamoreaux, P.E., Wilson, B.M. and Memeon, B.A. (eds.), *Guide to the Hydrology of Carbonate Rocks.* Paris: UNESCO, pp. 60-105, 116-130.
92. Fisher, D. (ed.) (1991) *Rules of Thumb for Engineers and Scientists.* Houston: Gulf Publishing Co., 242.pp.

93. Nordstorm, D.K. and Munoz, J.L. (1985) *Geochemical Thermodynamics.* Menlo Park, CA: The Benjamin/Cummings Publishing Co., 477pp.